Journal of Science: Advanced Materials and Devices 8 (2023) 100552

Contents lists available at ScienceDirect

Journal of Science: Advanced Materials and Devices

journal homepage: www.elsevier.com/locate/jsamd

Review Article

Electro-blown spinning: New insight into the effect of electric field and airflow hybridized forces on the production yield and characteristics of nanofiber membranes

Eman Elnabawy [a, *], Dongyang Sun [a], Neil Shearer [a], Islam Shyha [a, b]

[a] School of Computing, Engineering and the Built Environment, Edinburgh Napier University, Edinburgh, EH10 5DT, UK
[b] Production Engineering Department, Faculty of Engineering, Alexandria University, 21544, Alexandria, Egypt

ARTICLE INFO

Article history:
Received 1 October 2022
Received in revised form
3 January 2023
Accepted 28 February 2023
Available online 8 March 2023

Keywords:
Nanofibers
Electro-blown spinning
Hybridized forces
Large-scale production

ABSTRACT

Electro-blown spinning (EBS) is an emergent hybridized nanofibers formation technology. Recently, there has been a great interest in introducing this novel method for producing sub-micron, and nanofibers into several applications. For the first time, this comprehensive paper provides a detailed review for the EBS process, including working principle, operation parameters, nanofibers materials, setup modifications, and various applications. EBS is a hybridized nanofibers manufacturing process which combines between the solution-blown spinning (SBS) and electrospinning driving forces. The EBS process can produce outstanding spinning efficiency and superior nanofibers characteristics compared to the conventional spinning methods. Moreover, researchers have proved the efficient spinning capability of EBS with highly viscous polymers and its feasibility for large-scale production. Herein, we will show the potential of EBS to produce high-quality nanofibers and bring new insight into the process challenges and outcomes.

1. Introduction

It is known that nanomaterials have attracted researcher's interest in the previous decades for their extraordinary physical, chemical, and mechanical characteristics [1–5]. Nanomaterials have emerged as the most practical class of materials for industrial and domestic applications [6–9]. Many types of nanomaterials could be evolved according to their dimension and synthesis process [10–12]. Among all types of nanostructures, nanofibers are the most regarded form of nanomaterials because of their impressive surface area, tensile strength, and aspect ratio, in addition to their porous structure and feasibility of functionalization [13–15].

Nanofibers can be synthesized from natural or synthetic polymers in addition to ceramic, carbon-based, and semiconducting nanomaterials [16,17]. Among the several types of nanofibers materials, polymeric nanofibers have been heavily investigated for their wide diameter range (10–1000 nm), controllable pore size, and potential for biomedical implementation [18,19]. Various conventional spinning techniques have been used for polymeric nanofibers production [20,21]. This includes electrospinning [22], template synthesis [23], self-assembly [24], phase separation [21], melt blowing [25], and centrifugal spinning [26].

In recent years, researchers have developed those traditional insufficient fabrication techniques to become simpler, safer, and scalable [27]. Given this, more emerging strategies have been introduced for nanofibers formation, such as airflow bubble spinning [28,29], plasma-induced synthesis [30], CO_2 laser supersonic drawing [31], electrohydrodynamic direct writing [32], solution-blown spinning [33], and electro-blown spinning.

The uses and applications of nanofibers have been widely expanding due to their outstanding properties and superior surface-to-volume ratio. For example, nanofibers having diameters in range of 5–500 nm, possess a corresponding surface area of about 10,000 to 1,000,000 m^2/kg [34]. Such applications include filtration purposes [35], biomedical engineering [36], energy

Abbreviations: Al_2O_3, Aluminum oxide; AlCl3.6H2O, Hydrated aluminum chloride; ABS, Acrylonitrile butadiene styrene; BaTiO3, Barium titanate; BGn, Bioactive glass nanofibers; CeF3, Cerium (III) fluoride; CuO, Copper oxide; HA, Hyaluronic acid; HIPS, High impact polystyrene; LIB, Lithium-ion batteries; MnO_2, Manganese dioxide; MOF, Metal oxide framework; PVP, Polyvinylpyrrolidone; PVDF, Polyvinylidene fluoride; PTFE, Polytetrafluoroethylene; PS, Polystyrene; PMMA, Poly methyl methacrylate; PVC, Polyvinyl chloride; PVA, Polyvinyl alcohol; PAA, Poly(-acrylic acid); PAN, Polyacrylonitrile; PEDOT: PSS, Poly(3,4-ethylene dioxythiophene) polystyrene sulfonate; Si (OC2H5)4, Tetraethoxysilane; TcO^-_4, Pertechnetate.

* Corresponding author.
E-mail address: e.elessawy@napier.ac.uk (E. Elnabawy).

Peer review under responsibility of Vietnam National University, Hanoi.

https://doi.org/10.1016/j.jsamd.2023.100552

harvesting [37–39], cosmetics [40], protective clothing [41], and antibacterial scaffolds [42]. The enormous advance in nanofibers fabrication and functionalization has encouraged the industrial sector for providing large-scale production systems for membranes manufacturing [43,44], and replace the conventional hard, toxic, and non-degradable industrial materials with engineered polymeric nanofibers mats [45,46].

Reviews on nanofibers formation techniques have included a brief description of the EBS process or similar principal techniques [47]. Increasing the number of papers that have been published on this interesting technology (Fig. 1) reflects its efficiency in fabricating high-quality fibrous materials. The EBS process has been donated with (Electro-blown spinning) [48–53] (Electro-blowing) [54] (Gas/Jet/Air-assisted electrospinning) [55] (Electrode-assisted solution blowing) [56], and (Electrostatic-induction assisted solution blown spinning) [57]. All these terminologies share the same governing theory in different working mechanisms, which shows the growing attention to the hybridized EBS technology.

EBS is a hybrid process which combines the powerful forces of an electric field and high pressurized gas into one efficient integrated setup (Fig. 2). This novel technology introduces more advanced features to overcome the limitations of separate processes such as the low production rate of electrospinning and jet instability of SBS. Herein, we provide an overall view of EBS including, the working mechanism, current materials, setup modifications, and conducted applications. This paper presents the latest research on the EBS nanofibers membranes and covers their potential for industrial applications.

2. Role of hybridization in electro-blown spinning

Researchers divided the nanofibers formation processes into electrospinning and non-electrospinning [58]. Electrospinning-driven processes provide an electrical potential to facilitate the formation of nanofibers through an electrostatic force [59]. On the other hand, non-electrospinning processes provide an alternative driving force such as centrifugal force [60], pressurized gas [61], high-temperature gradient [62], or chemical bonding [63]. Among all conventional and emergent spinning processes, electrospinning and solution blown spinning have been widely studied and developed for diverse applications [64]. Ahmed et al. compared the difference between the two processes in terms of nanofiber diameter, surface area, and scalability. It was found that the electrospinning nanofibers had a larger diameter and smaller surface area, while the SBS nanofibers attained higher density and production yield [65]. The role of hybridization between the electric field and pressurized-air forces was firstly developed by Um et al., in 2004 who proposed the preparation of high molecular weight hyaluronic acid (HA) through an electric-field assisted air blowing

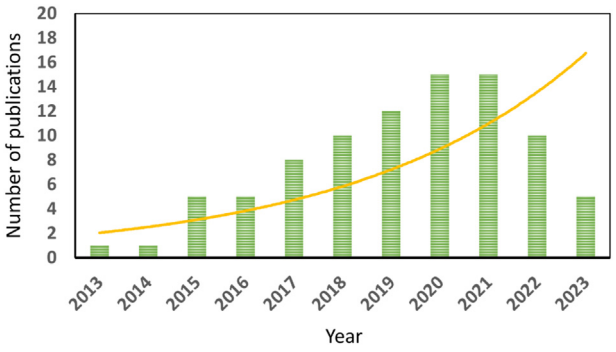

Fig. 1. Number of publications on the EBS process, updated until January 2023.

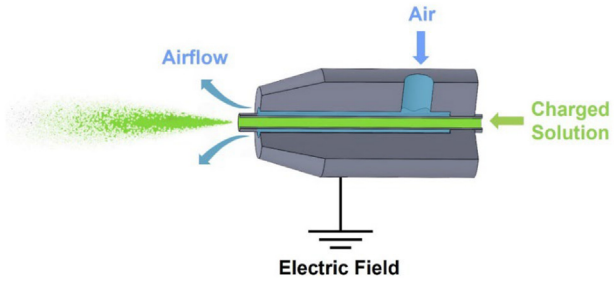

Fig. 2. Schematic drawing for the EBS hybrid forces.

spinning setup [66–68]. After that, Lin et al. successfully prepared polyvinylidene fluoride (PVDF) nanofibers via EBS in 2009, and thoroughly studied the influence of gas flow on the crystal and morphological structures of the produced membranes [69].

2.1. Electrospinning

For many decades, electrospinning considered the most common and attractive process for nanofibers formation due to its simple operation, low cost, nanofiber diameter control, ability to fabricate aligned and randomly oriented nanofibers, and process continuity. The electrospinning setup is composed of three main parts, as shown in Fig. 3; a syringe pump that ejects the polymer solution at a specific feeding rate, A power supply that is applied to the spinning nozzle to generate an electric field between the nozzle and the collector for the formation of nanofibers, and a grounded static or dynamic collector to receive the produced nanofibers [70]. The working principle of electrospinning is based on electrifying the polymer solution through a high electric potential to form stretched solution jet which is called “Taylor cone” [71]. The extruded jet flies in the direction of the collector where the solvent evaporates, and nanofibers accumulate into layers. Several modifications were lately provided to the typical electrospinning setup. Some modifications can involve either a change in the nozzle design or collector material [72,73], while others rely on subjecting additional assisted force to the high electric field [74].

Electrospinning has a broad variety of applications including supercapacitors [76], biomedical devices [77], tissue engineering [78,79], piezoelectric nanogenerators [80], and air filtration [81,82]. Zhang et al. demonstrated the coupling performance of triboelectric-piezoelectric polyvinylidene fluoride/Barium titanate ($PVDF/BaTiO_3$) nanofibers membrane and found that it had a remarkable coupling state of 105.6 $\mu C\ m^{-2}$, which is double the pristine PVDF reference [83]. Comparatively, kumar et al. showed the effect of zinc oxide (ZnO_2) nanoparticles addition on the piezoelectric performance of electrospinning poly vinylidene fluoride-trifluoroethylene (PVDF/TrFE) self-powered sensor [84]. It was observed that the output voltage significantly enhanced by increasing the ZnO_2 concentration up to 2.52 V with a current density of 20.8 μA. Conjugate electrospinning was recently used for yarns production [85–87]. The process is based on the operation of two high voltage power supplies with different polarities connected to separate spinnerets wherefrom the fibres are ejected and collected onto a drum. Xue et al. presented an integrated PVDF/nylon core shell yarn structure with high piezoelectric properties for wearable sensing applications [87]. The piezoelectric outputs of the yarn showed a remarkable stability after 800 s fatigue test with a maximum current of 32.8 nA at a frequency of 4 Hz and maintained cycle stability for more than 3200 cycles.

Due to the COVID-19 pandemic, the high demand for efficient face masks that could prevent infectious viruses became an

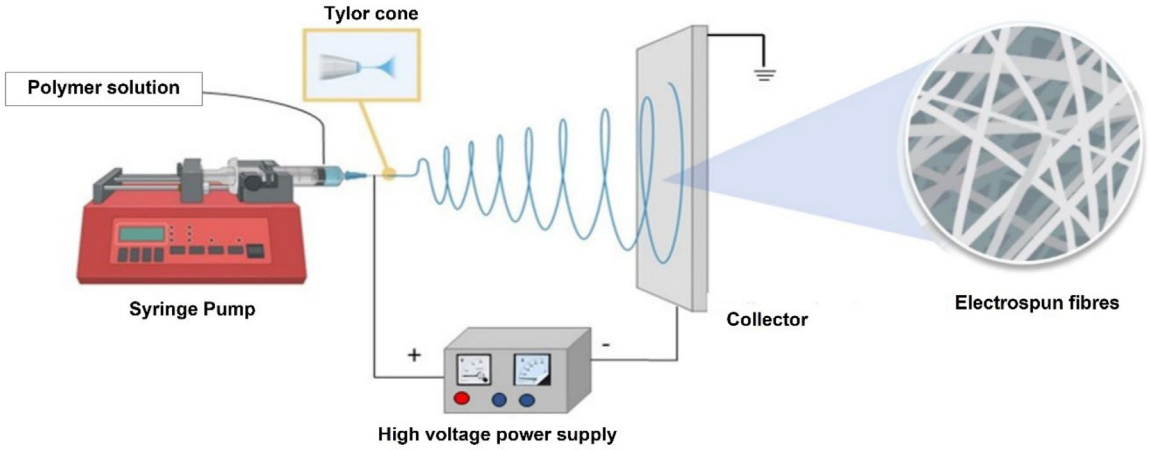

Fig. 3. Schematic drawing for electrospinning setup [75].

immediate focus for the research and industrial sector. T. Le et al. recently fabricated a novel PLLA (Polylactic acid) piezoelectric self-cleaning face filter mask with a long lifetime material decomposition of up to 5 weeks [88]. The PLLA scaffold showed high filtration efficiency up to 99% for $PM_{2.5}$ and 91% for $PM_{1.0}$, respectively in addition to the durability and recyclability of the filtration mask.

Regardless of the advantages of electrospinning, many process limitations can hinder the applicability of electrospinning nanofibers membranes. The most common drawbacks of the electrospinning process are the safety hazards of the high electric field, difficulty to obtain 3D structure nanofibers mat, low production rate, and the use of halogenated and toxic solvents [89]. Recent studies mentioned the effect of solvent retention in electrospinning on achieving efficient bio-fabrication using living cells. Nam et al. tested the solvent retention of polycaprolactone (PCL), gelatine, and PCL-gelatine blend nanofibers during the electrospinning process and found that most of the nanofiber membranes contained as much as 1600 ppm of remaining solvent which badly affected the cell viability [90].

2.2. Solution-blown spinning

SBS is a maturing spinning process in which a high yield of continuous nanofibers can be synthesized under the effect of pressurized gas. As shown in Fig. 4a, the SBS concentric nozzle combines two parallel fluid streams of polymer solution surrounded by gas flow to generate a widely distributed jet [91,92]. The physical principle of the SBS process follows Bernoulli's equation which states that any change in pressure can be converted into kinetic energy. Accordingly, at the tip of the nozzle, the high pressurized gas stream drops into the atmospheric pressure generating shearing force at the gas/solution interface [92]. With increasing the gas pressure, this shearing force overcomes the polymer's surface tension, and the solution jet is ejected from the nozzle in the direction of the gas stream (Fig. 4b).

The SBS process has attracted the researcher's interest over the previous decade for its safe, and simple operation in addition to its capability for large-scale production. The SBS process is more favourable for industrial applications because of its high scalability and deposition rate which is 10 times faster than conventional electrospinning [93]. The demand for SBS nanofibers, particularly for biological purposes is hugely increasing due to the rapid biological scaffold generation and custom in situ materials fabrication (Fig. 4c and d). However, there are some reported disadvantages to the conventional SBS process [94], such as the uncontrolled deposition of nanofibers, nozzle clogging, and jet instability [95]. Li et al. observed the formation of beads for SBS alumina nanofibers due to the jet instability and blockage of the nozzle's tip during the spinning process [52]. While Ray et al. reported that the nozzle protrusion length is hampering the airflow, which causes disturbance to the produced jet and nanofibers discontinuity [96].

Many attempts were introduced to overcome the limitations of the SBS process. Kolbasov et al. fabricated a hollow vacuum-connected drum with a metallic mesh surface to minimize the wasted nanofibers in the collection chamber [97]. The vacuumed collector has significantly facilitated the adhesion of nanofibers which consequently enlarged the area of the produced sample. Several studies demonstrated the effect of nozzle design on the morphological structure of the generated nanofibers. Han et al. presented a computational fluid dynamics (CFD) study to observe the effect of nozzle diameter and needle protrusion length on the diameter of chitosan/polyethylene oxide PEO nanofibers [98]. The calculations confirmed that a larger internal nozzle orifice generates larger solution droplets which in return increase the nanofiber diameter. Similarly, a very small orifice produces higher gas velocity and fine nanofibers diameter. More investigation into the effect of the process temperature and air density was conducted by Atif et al. using the k-ε turbulence model through CFD simulation to describe the fluid flow characteristics under a turbulence condition [99]. The results showed that by increasing the air pressure to 5 bar, the process temperature dropped from 25 to 22 °C following the Joule-Thomson effect. This temperature drop acted as additional stress on the extruded solution jet leading to the formation of unstable jets, and another driving force was required for steadily and constantly stretching. The previous theoretical investigation was experimentally confirmed by Elnabawy et al. who studied the effect of increasing the SBS gas pressure from 2 to 5 bars on the morphological structure of PVDF nanofibers. The resulting data revealed that increasing the gas pressure stimulates the nanofibers to overlap in form of stacking bundles [100].

2.3. Hybridized electro-blown spinning

EBS is a merged process between the electrospinning and SBS driving forces. The EBS setup is composed of a compressed air source, high electric field, SBS concentric nozzle, syringe pump, and rotating drum collector (Fig. 5) [101]. The EBS process can produce a wide range of nanofiber diameters from 10 μm to 68 nm [52,102]. The working mechanism of EBS is based on introducing combined forces of electric field and airflow onto the extruded polymer

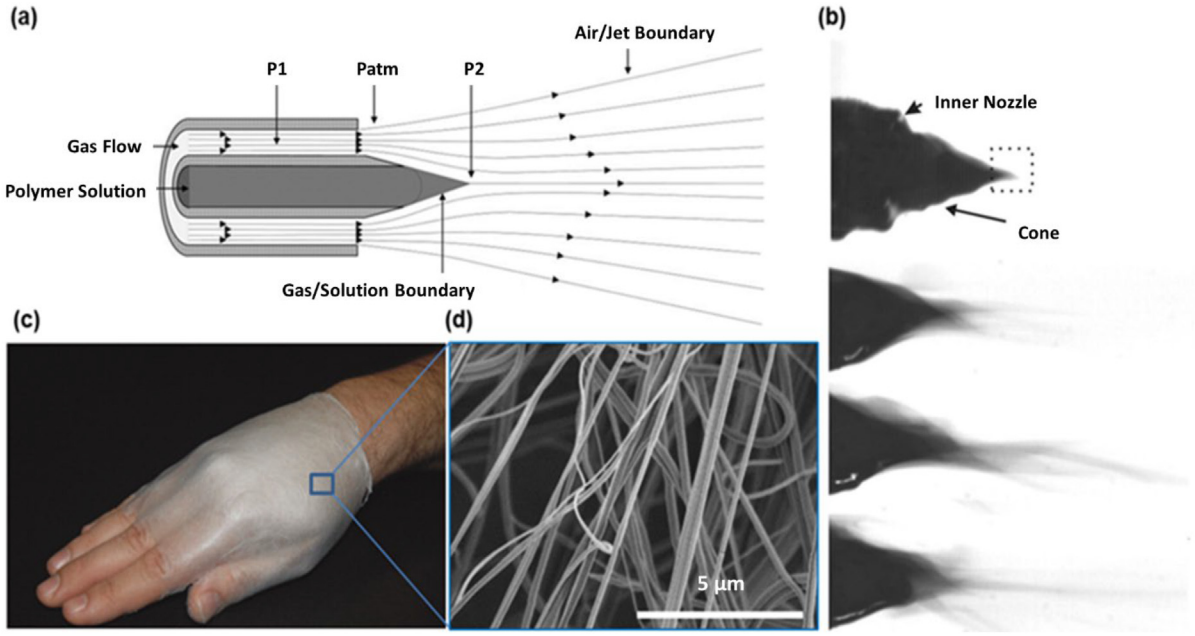

Fig. 4. (a) Working principle of the SBS process, (b) the structure of polymer droplet under the effect of pressurized air (c & d) formation of NFs layer, and the corresponding SEM image [92].

solution at the spinneret tip. Typically, the dominating force near the nozzle's tip is the pressurized airflow, while with increasing the nozzle-to-collector distance, the electrostatic repulsive force starts to control the spinning process generating more stable solution jets [50]. The synergistic effect of a high electric field and compressed blown flow offers the EBS remarkable efficiency in terms of production rate and spinning speed [103].

The most interesting feature of EBS is the high solution jet stability due to the sufficient drafting forces of electric field-assisted with airflow. Thus, the polymer feeding rate could reach 30 ml/h [50]. Accordingly, considerable thick nanofibers mat of a few microns can be obtained promptly with homogenous distribution and extremely fine diameter. In addition, the resulting nanofibers morphology is more controlled and uniformly distributed which is hard to achieve using the conventional SBS disturbed jet that is always combined with solution accumulation and spinneret blockage. A brief comparison between electrospinning, SBS, and EBS, in terms of advantages and disadvantages, is presented in Table 1.

Researchers found that the addition of an electric field to the conventional SBS process significantly enhanced the stretching and traction of the extruded jet [52,54,107]. Moreover, it was found that

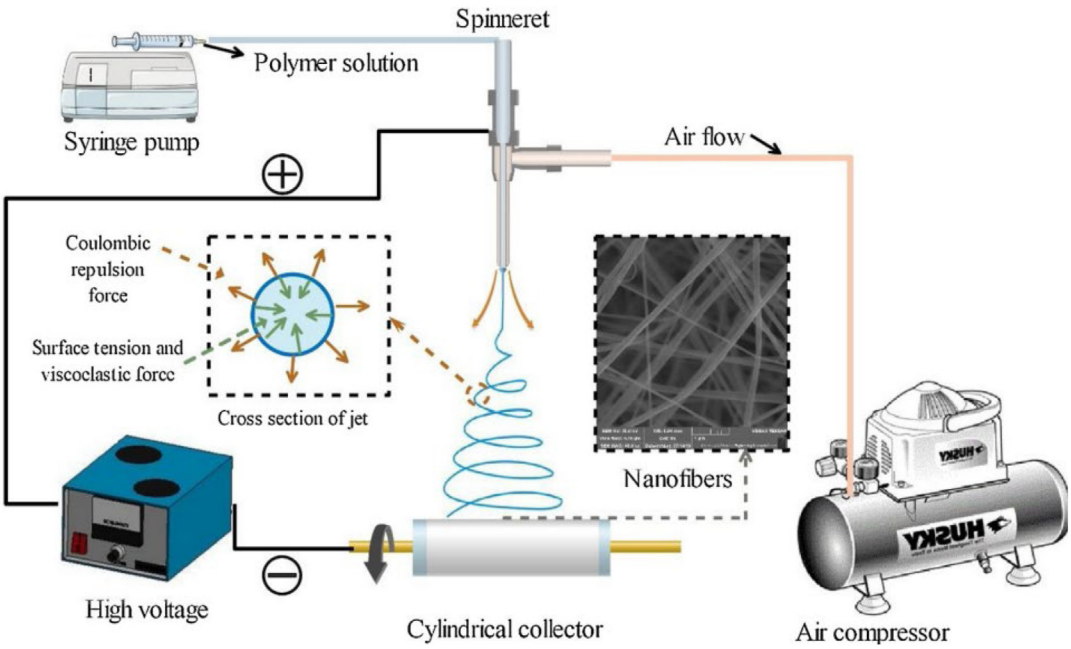

Fig. 5. A Schematic for the electro-blown spinning setup [101].

Table 1
Advantages and disadvantages of the Electrospinning, SBS, and EBS processes.

Method	Advantages	Disadvantages	References
Electrospinning	• Inexpensive • Simple operation	• Hazard of high voltage • Limitation with conductive polymers	[77,89,104,105]
SBS	• Large-scale production • Safe • Wide range of materials • Suitable for industrialization prospect	• Uneven distribution of nanofibers • Easy folding and bending of nanofibers • Jet instability • Nozzle clogging • Formation of bundles at high air flow	[91,92,106]
EBS	• Fine & uniform nanofibers formation • Stable solution jet • Suitable for highly viscous polymers	• Controlling multiple parameters simultaneously	[48,50]

the produced nanofibers became finer, uniform, and homogeneously distributed. Cao et al. presented the difference in diameter and jet stability of silk/graphene nanofibers membranes prepared via the three spinning processes [50]. As shown in Fig. 6(d), the SEM images of the EBS nanofibers had the smallest diameter of 454 nm, compared to the electrospinning and SBS which showed larger diameter of 644 nm and 613 nm, respectively (Fig. 6e and f). Furthermore, the extruded solution jet of EBS had a very stable stage with an estimated length of 17 mm and a spreading angle of 16° (Fig. 5a) compared to the randomly oriented jet of electrospinning and the unstable jet of SBS.

Liu et al. also explained the effect of introducing an electric field in separating the polyamide SBS bundled structure into random-oriented single nanofibers by applying 10 kV to the spinning nozzle [108]. As shown in Fig. 7a, multiple single nanofibers were stacked together in form of bundles due to the combined effect of turbulent airflow and fusion of solution jets before complete solvent evaporation [109]. However, when an electrostatic force incorporates with the pressurized air, stable confined jets can be produced, and the repulsion of electrical charges prohibits the formation of bundles (Fig. 7 (b)). For the mentioned reasons, the EBS process considers more efficient compared to SBS and electrospinning.

Different structures and morphologies of EBS nanofibers were recently introduced to obtain unique properties for specific applications [110–112]. Titanium dioxide/Silicon dioxide (TiO_2–SiO_2) submicron fibres covered with TiO_2 nanorod layer was prepared via EBS for Strontium (Sr^{2+}) uptake [112]. It was observed that the hydrothermal reaction time and TiO_2 content had a predominant effect on the density, length, and diameter of nanorods. Noticeably high nanorods length of 700 nm was detected at 6 h hydrothermal time, in addition to the formation of star-shaped and branched rods structures onto the fibres surface. All the pristine and modified submicron fibres showed excellent adsorption capability >90%. However, the hydrothermally modified fibres with TiO_2 nanorods had superior uptake with highest kd value of 3490.000 ml. g^{-1}. This superior uptake for the modified fibres is evidently based on the large surface area of TiO_2 nanorods. Another nanostructure of amorphous mesoporous silica fibres was prepared by EBS for poly (methyl methacrylate)/tetraethoxysilane mixture (PMMA/TEOS) [111]. The obtained fibres showed nanometre sized pores of 20 nm which can be suitable for various applications such as catalysis, and biomolecules separation. Novel and hybrid structure of acrylonitrile-butadiene-styrene (ABS) nanofibers manufactured via EBS coated with hydrophobic polystyrene (PS) nanoparticles via electro-spraying was thoroughly investigated for direct contact membrane distillation (DCMD) [110]. The mounted PS beads on the electro-blown ABS nanofibers layer achieved high surface roughness with enhanced hydrophobicity from 137.9 to 157.8°. Moreover, the water liquid entry pressure (LEP) of the fabricated ABS/PS membranes was incredibly improved 4.1 times compared to the neat ABS membrane. Excellent DCMD performance with significant water flux and salt rejection was also detected due to the hydrophobic nature PS nanoparticles.

Despite the considerable reported advantages of the EBS process in terms of production rate and high-quality nanofibers manufacturing. Several disadvantages to EBS have been recently founded. For example, the quite high applied electric field, process interruption due to nozzle clogging, difficult electric insulation and coupling of working distance to applied voltage [113]. A subsequent patent by Bryner et al. enhanced the EBS process by directly applying the voltage to a pair of electrodes located parallel to the

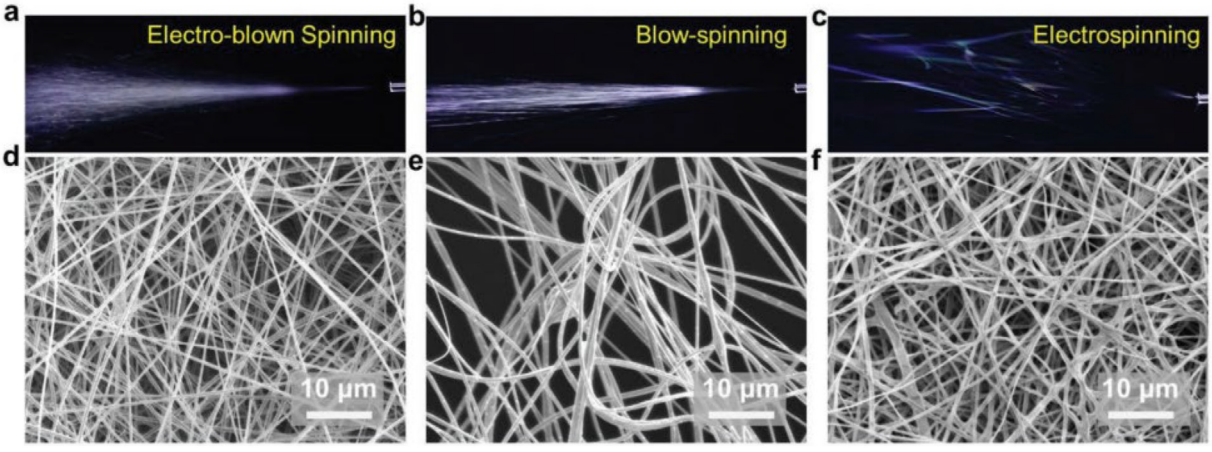

Fig. 6. Snapshots for the generated solution jet and resultant SEM image of Electrospinning (a & d), SBS (b & e), and EBS (c & f) [50].

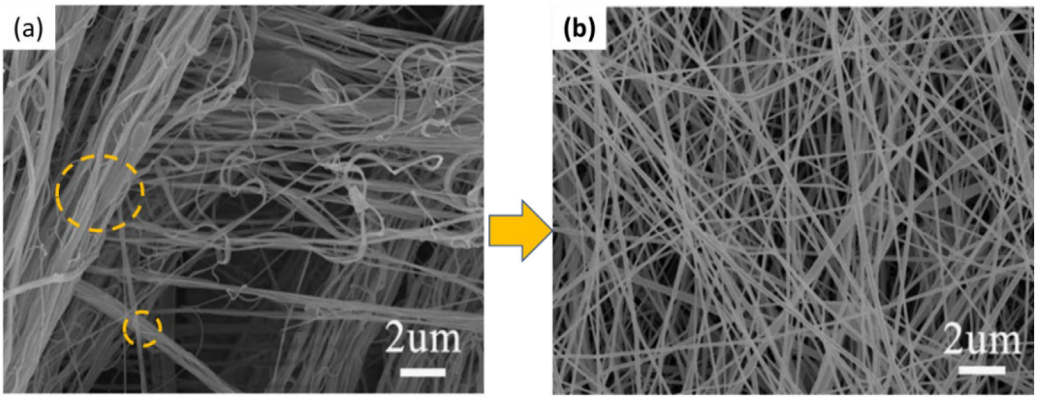

Fig. 7. SEM images for (a) the SBS bundled nanofibers, and (b) EBS single-oriented nanofibers (96).

surface of a grounded spinneret [114], which significantly improved those disadvantages caused by the conventional voltage application method. Based on the previous study, Chu and co-workers developed a multi-nozzles EBS setup for large scale production of hyaluronic acid nanofibers [115]. A five times higher throughput in each nozzle of this modified EBS could be achieved compared to that of the conventional EBS.

3. Parameters affecting the electro-blown spinning process

Several parameters can affect the diameter and morphological structure of the EBS nanofibers [107,116,117]. As seen in Table 2, these variables can be classified into three main categories: (1) polymer solution influence, (2) process parameters influence, and (3) ambient influence.

3.1. Polymer solution parameters

The intrinsic properties of polymer solution including polymer concentration, viscosity, surface tension, and solvent evaporation rate have a pronounced effect on the diameter of nanofibers as well as their homogeneous distribution. Previous studies proved that the diameter increases linearly with polymer concentration [118]. As shown in Fig. 8 [107], Choi et al. reported that the diameter of Polyvinylpyrrolidone (PVP) nanofibers was remarkably increased from 678 nm to 2400 nm by increasing the polymer concentration from 8 wt.% to 12 wt.%. Zhou et al. also explained the effect of PVP addition on increasing the viscosity of $CeO_2/CuO/Al_2O_3$ co-solution and the generated nanofiber diameter [119,120]. The results showed a significant increase in diameter from 1.5 μm to 4 μm with increasing the PVP content from 0 to 14%. Theis noticeable increase in diameter with higher polymer concentration is ascribed to the effect of solution viscosity in evolving higher intermolecular entanglement through the polymer chains and producing higher surface tension which resists the applied driving forces [119].

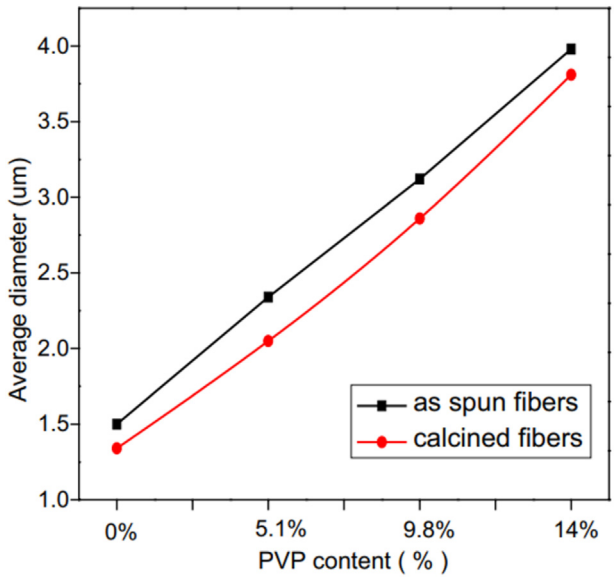

Fig. 8. Effect of increasing the PVP solution concentration on EBS nanofibers diameter [107].

3.2. Process parameters

Process parameters such as gas pressure, electric field, injection rate, and nozzle-to-collector distance have a significant effect on the produced nanofiber diameter [121]. Zheng et al. demonstrated the effect of pressurized air on the PEO nanofibers diameter and

Table 2
Variables affecting the morphological structure and diameter of the EBS nanofibers.

Parameters		Morphology & nanofibers diameter	Ref.
Polymer Solution	Concentration	High solution concentration leads to higher viscosity & large nanofibers diameter.	[117]
Process Parameters	Feeding rate	Excessive flow rate leads to solution leakage, nozzle blockage & large nanofibers diameter.	[107]
	Voltage	Increasing applied voltage produces continuous, fine & more uniform nanofibers distribution.	[48,128]
	Air pressure	Increasing air pressure generates small nanofibers diameter & high production yield.	[48,107]
	Working distance	Increasing working distance improves the possibility of solvent evaporation & thus generates a small nanofiber diameter	[122]
Ambient Parameters	Humidity	High humidity leads to quick nanofibers solidification & generates a small diameter	[129]
	Temperature	Increasing ambient temperature leads to high nanofibers continuity, better flexibility & narrowed diameter distribution	[54]

found that with a slight increase in air pressure from 0.01 to 0.015 MPa, the diameter declined from 3284 nm to 2701 nm [122]. Ju et al. reported the same findings for Polytetrafluoroethylene/Polyvinyl alcohol (PTFE/PVA) nanofibers which showed a dramatic decrease in nanofibers diameter from 1 μm to 400 nm when increasing the air pressure from 0.06 MPa to 0.14 MPa [48]. Increasing the pressure is accompanied by a rapid increase in air velocity, which promotes stronger shearing force at the gas/liquid interface and accelerates solvent evaporation, leading to a noticeable reduction in nanofibers diameter. While further pressure increase can negatively affect the spinning process through the formation of non-continued stacked bundles [107]. Moreover, gas pressure cannot only affect the diameter, but also the crystal structure of the synthesized nanofibers. Lin et al. investigated the effect of process pressure on the crystal structure of PVDF gas-jet/assisted electrospinning nanofibers. The Fourier transform infrared spectroscopy (FT-IR), and X-Ray diffraction (XRD) results indicated an improved crystallinity and β phase content for the high-pressurized gas nanofibers mats due to the influence of gas drawing force in inducing a conformational change to all-trans (TTTT) planar zigzag dipoles which then promotes the formation of β-phase crystal structure [69]. Researchers also discovered that gas pressure is a key factor in lowering the bead density [118]. As shown in Fig. 9a, Hsiao et al. found that by increasing the air pressure from 0 to 0.5 MPa, the number of beads noticeably declined from 80% to 5%, while the nanofiber diameter showed a slight decrease from 0.17 to 0.12 μm before it climbs again to the initial diameter with further pressure increase (Fig. 8b). A similar trend was reported by Zhou et al. who confirmed that increasing the gas pressure up to a certain limit can remarkably shrink the nanofiber diameter, while any additional pressure will lead to a larger diameter due to the lack of nanofibers stretching [107].

The electric field in the EBS process functions as a supplementary force to airflow, facilitating the traction and stretching of the fluid jet stream, and allowing for the generation of fine and uniform nanofiber diameters. Ju et al. noticed an inverse correlation between the voltage and nanofibers diameter with increasing the applied voltage from 30 to 45 kV, and a significant drop in diameter from 1 μm to 529 nm resulted [48]. Similarly, Zhou et al. demonstrated that the average nanofibers diameter of $CeO_2/CuO/Al_2O_3$ was reduced from 3.85 to 3.0 μm when the voltage increased to 40 kV [107]. However, increasing the electric field over a specific limit can be considered a source of hazard. The safety limit for DC electric field intensity that can be allowed for the human body should be lower than 5 kV/m which is corresponding to a maximum current of 25 mA [123]. However, the EBS process introduces an applied voltage of 10–50 kV through a working distance of 10–100 cm between the syringe and collector. When the electric field strength increases to 20–30 kV/cm, the surrounding air molecules will be ionized leading to a serious risk of touching the setup parts. Accordingly, the electric field intensity for the electrospinning and EBS processes should not exceed the safety limit of 20–30 kV/cm [105].

Other crucial process parameters that can strongly affect the generated nanofiber diameter are the polymer feeding rate and nozzle-to-collector distance [124]. It was previously reported that the diameter of the nanofibers increases proportionally with increasing the injection rate up to a certain extent to avoid wasting raw materials [52]. Zhou et al. found that when the polymer feeding rate exceeds 40 ml/h, the needle will be jammed causing disturbance to the spinning process and leakage of polymer solution [107]. Nozzle-to-collector working distance is one of the essential parameters that should be optimized according to each spinning process. Scientists ascertained that a short working distance prevents solvent evaporation and hinders nanofibers formation, while the too-long distance may cause random deposition and waste of the produced nanofibers into the spinning cabinet [56]. He et al. demonstrated that the minimum working distance that can allow the solvent to evaporate to form a fibrous structure is 9 cm, However, with increasing the distance up to 50 cm more uniform and homogeneously oriented nanofibers were detected [125]. For clarification, the observable effect of low and prominent levels of each process parameter on the produced nanofiber diameter is shown in Fig. 10 (a-c).

3.3. Ambient parameters

Atmospheric parameters such as humidity and air temperature have a great influence on the produced nanofiber diameter. Pokorny et al. exhaustively studied the effect of the latest factors on the diameter and production yield of HA and PEO. They observed a slight increase in the weight of the produced nanofibers membrane from 110 mg to 140 mg by increasing the humidity from 24 to 35%, while the diameter was decreased from 140 to 85 nm [126]. The reason behind this change is the effect of humidity on inhibition of the solvent evaporation rate leading to slow solidification and thinner nanofibers diameter formation [127]. Regarding the air temperature impact, the authors found that heating the airflow to 31 °C caused a further increase in nanofibers production from 141 mg to 264 mg over 30 min, which is almost 1.9-fold the

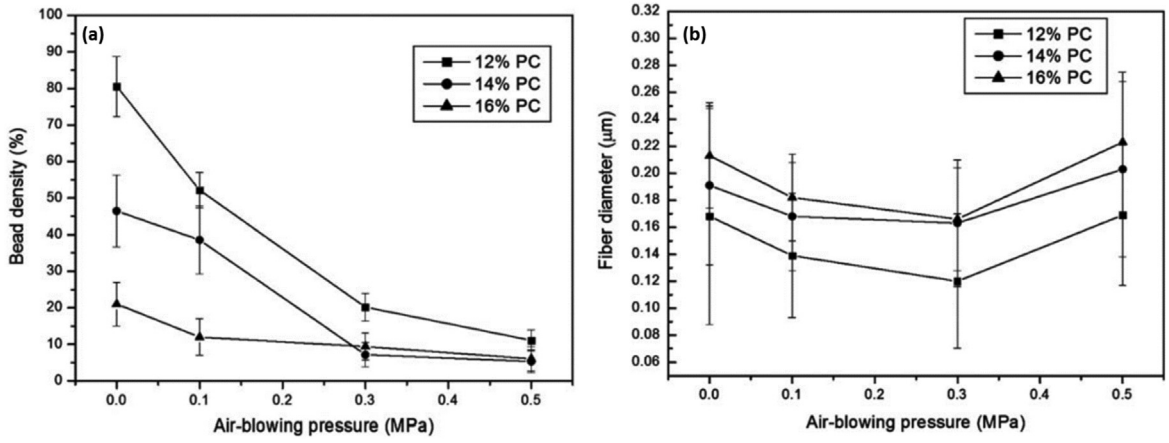

Fig. 9. Effect of air-blowing pressure on (a) beads density, and (b) nanofibers diameter of polycarbonate nanofibers [118].

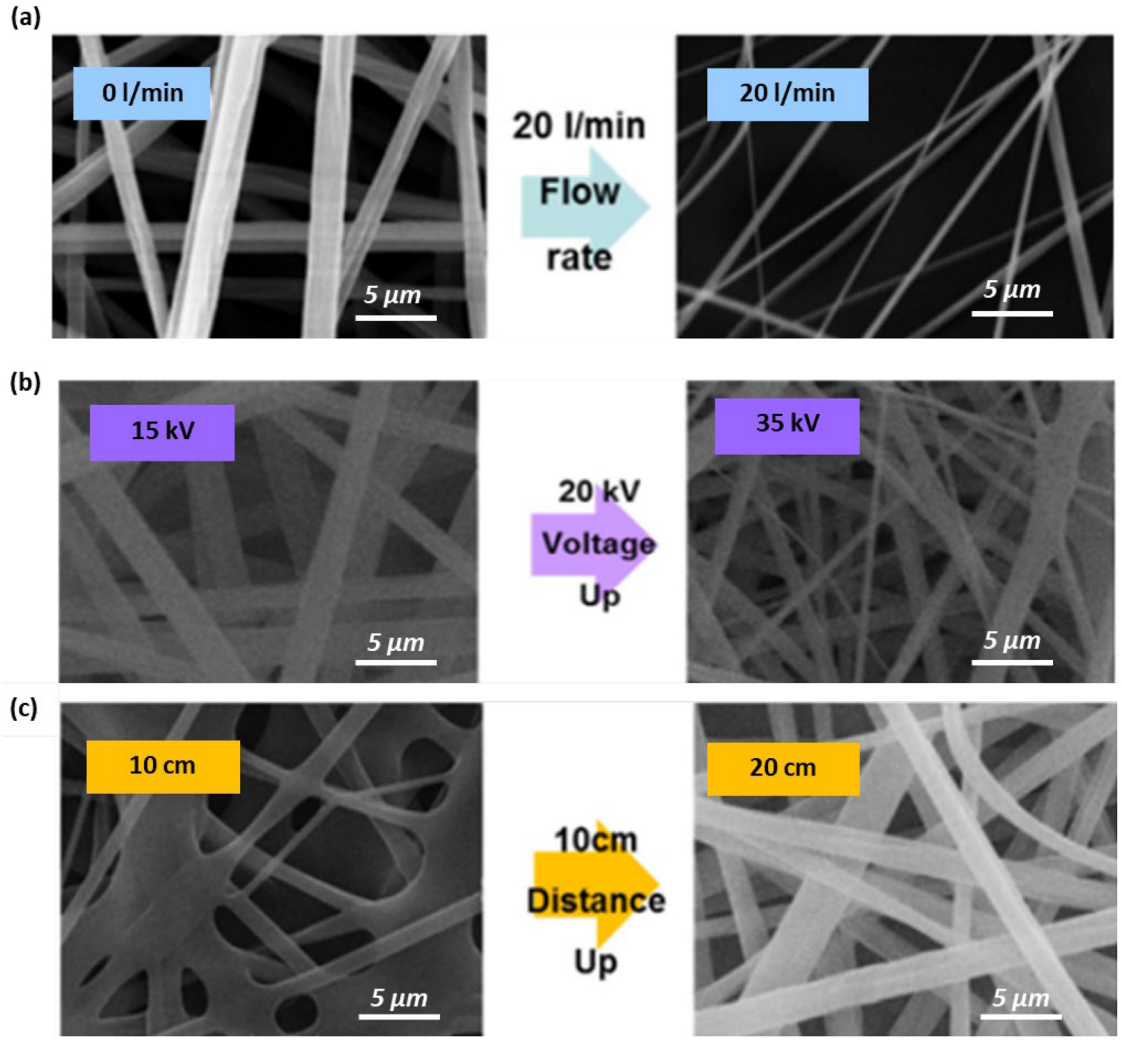

Fig. 10. SEM images for the effect of low, and high (a) airflow rate, (b) electric field, and (c) working distance on the produced EBS nanofibers diameter [117].

unheated airflow. This can be explained by the effect of heated airflow on increasing the solution temperature leading to higher thermal motion for individual polymer chains and lower viscosity resulting in a thinner diameter [126].

4. Materials for electro-blown spinning nanofibers

The concept of the EBS process was initiated by Um et al. who proposed the preparation of high molecular weight hyaluronic acid (HA) for the first time through an electric-field assisted blowing spinning setup [66,67]. The study reported the effect of applied voltage and heated airflow via air distributor nozzle on the generated nanofibers diameter. They recognized that by increasing the airflow up to 150 ft^3/h and applying a high electrostatic charge, there was a chance to produce low-density non-continuous nanofibers, but it was not adequate to achieve a consistent production yield of high-quality nanofibers. The study discovered that the most predominant factor in the formation of homogenously continuous non-woven nanofibers was the temperature of the blown air, and the best nanofibers quality was produced at a blown air temperature of 57 °C. Following that, several polymeric materials which can be hardly spinnable through the conventional spinning techniques were employed in the EBS process [130–144]. Table 3 summarizes some of the reported polymeric nanofiber materials introduced through the EBS process and their corresponding nanofiber diameter. As seen in Table 3, various materials were studied with a wide range of operating parameters including polymer concentration, gas pressure, applied voltage, injection rate, and nozzle-to-collector working distance.

5. Modifications of the electro-blown spinning setup

Many design modification attempts have been made to the current EBS setup to minimize the significant risk associated with applying a high electric field. A novel model of cylindrical-electrode-assisted SBS setup was recently studied by connecting a high-voltage power supply to a hollow metallic cylinder opened from both sides as shown in Fig. 11(a). Through the electrode cylinder, PEO nanofibers jets flow from the SBS nozzle to the grounded plate collector under an electrostatic induction force [56,128,150]. The authors thoroughly investigated the impact of polymer injection rate, air pressure, electrical voltage, cylinder diameter, needle-to-cylinder distance, and length of the cylinder on generated nanofibers diameter and surface porosity. They found a considerable decrease in diameter with increasing feeding rate, pressured gas, cylinder length, and applied voltage. In contrast, increasing the cylinder diameter and needle-to-cylinder distance provided a noticeably larger diameter. Tang et al. have also demonstrated the

Table 3
EBS operating parameters and the corresponding nanofiber diameter for different polymeric materials.

Materials	Concentration (wt.%)	Pressure (MPa)	Voltage (kV)	Feed Rete (ml/h)	Working Distance (cm)	Nanofibers Diameter (nm)	Ref
$AlCl_3 \cdot 6H2O/Si(OC_2H_5)_4$/PVA	8	0.2	30	80	100	2700	[52]
PVA/PTFE	10	0.1	40	20	100	443–634	[53]
PVA/PTFE	10	0.6–0.14	30–45	20	100	400–1000	[48]
CeF3– PCNF	16.7	0.1	40	20	100	320–390	[145]
PVP	8–12	0.2	15–35	28.5	10–20	170–3228	[116]
PEO	7	0.01	12	0.2	100	657	[56]
HA	2.5	N/A	40	0.3–0.6	9.5	74	[54]
PVDF/modacrylic	13	0.2	25	5	30	211–384	[146]
SiO_2/PTFE	10	0.1	40	N/A	80	448–650	[147]
$CeO_2/CuO/Al_2O_3$	0–6	0.05–0.2	10–40	30	80	3000	[135]
PA-66	15	0.7	20	500	65	116	[148]
Silk/Graphene	N/A	0.1	25	5	35	454	[50]
PAN	12	0.1–0.2	5–25	5–15	20–60	110–180	[57]
PVDF	12	0.1	0–30	5	30	408–424	[149]

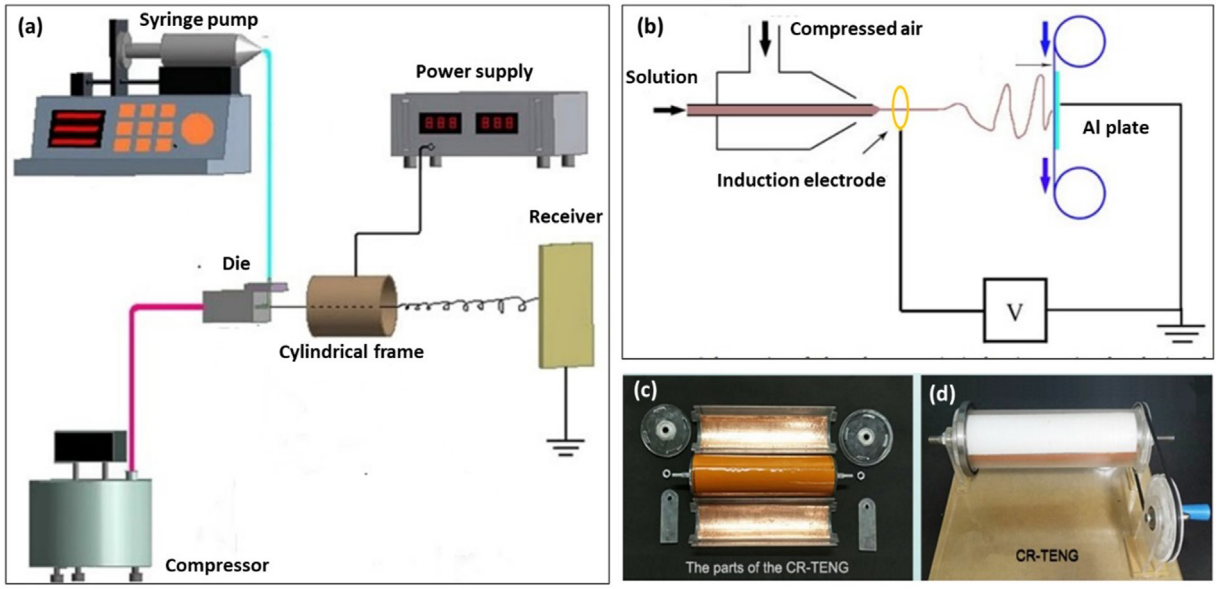

Fig. 11. (a) Schematic description of cylindrical electrode assisted SBS setup [56], (b) electrostatic induction assisted SBS setup [57] (c & d) triboelectric nanogenerator rotating cylinder [51].

effect of induced electric field on the production of PAN nanofibers via the EBS process [57], see Fig. 11(b). A circular copper induction electrode has been located 5 mm away from the SBS nozzle tip and connected to the electric field source where induction voltage was applied. It was observed that increasing the induced electric field up to 25 kV significantly promoted the separation of stacked bundled into single nanofibers with a diameter of 117 nm at a fixed air pressure of 0.1 MPa.

A recent study fabricated a new triboelectric nanogenerator rotating cylinder that could functionalize as both a high-voltage source and nanofibers receiving collector [51]. The innovative electrified cylinder of the modified driven EBS system has achieved an output voltage of 6.250 kV which could preserve about 21% of conventional high-voltage power supply consumption. The authors successfully synthesized nanofibers from varied materials including PEO, PAN, and PVA with a minimum diameter of 2.3 μm. Furthermore, the modified EBS system can efficiently produce several micron thick membranes within a few seconds of processing, which assures its capability for large-scale production. He et al. proposed an experimental and CFD modelling analysis for a new high-pressure air-jet split electrospinning process to increase the mass production of polyacrylonitrile (PAN) nanofibers [125]. The air-jet splitter setup could generate wider jet distribution by inserting a 700-mesh filter screen onto the nozzle tip (Fig. 11a). During the experiment, the airflow was transported to the nozzle at a pressure of 0.8 MPa, and the PAN solution ejected at a fixed rate of 1500 ml/h. The mesh filter screen divided the spinning solution into about 20 μm size droplets which were then split into smaller ones with the aid of high-pressure airflow and an electric field of 30 kV. Moreover, they studied the effect of nozzle-to-collector working distance (Fig. 12b) and charging the whole nozzle body on the production yield and nanofibers diameter. The obtained results proved that with increasing the working distance by more than 9 cm, the electric field forces started to dominate producing wider jet distribution with a cone angle of 19° (Fig. 12e), larger deposition area, and higher nanofiber density (Fig. 12d) compared to the conventional electrospinning process (Fig. 12c). Furthermore, charging the whole nozzle body reduced the nanofiber diameter from 335 to 171 nm due to the stronger electric field intensity.

Vortex spinning is a pneumatic spinning technique to produce yarn structure [151,152]. Tian et al. demonstrated for the first-time a vortex electrospinning setup (Fig. 13) inspired by the DNA helical

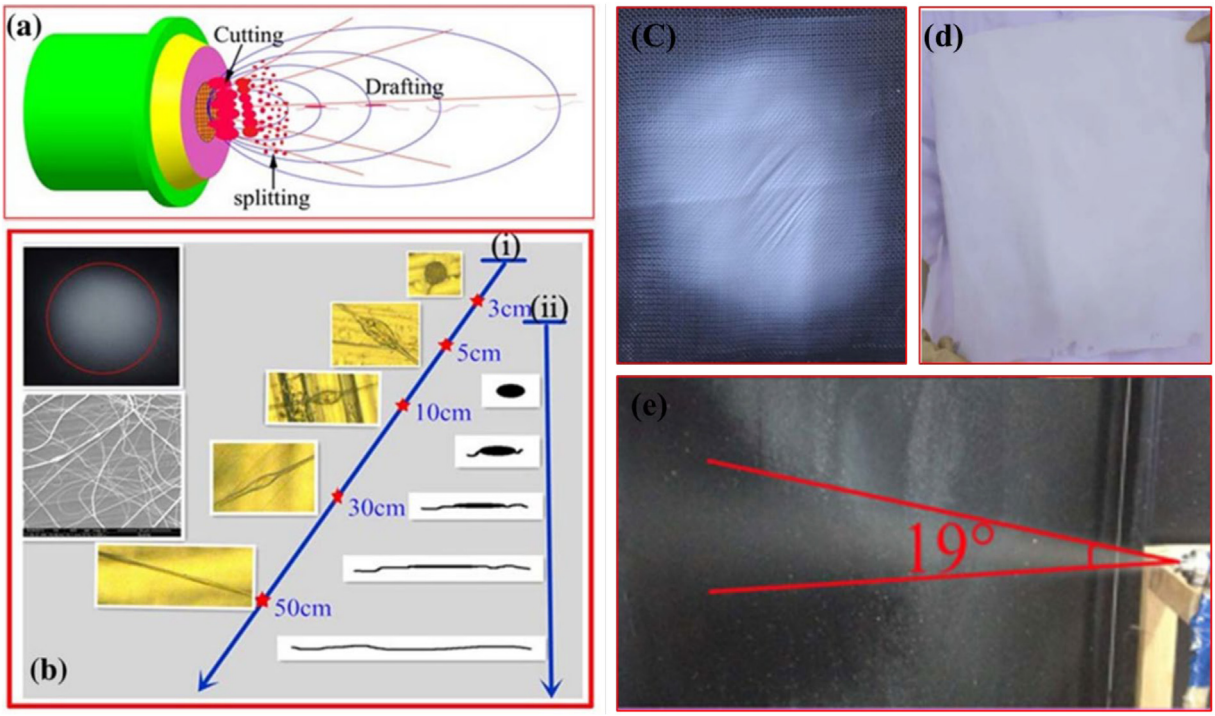

Fig. 12. (a) Schematic drawing for splitting the solution jet through the 700-mesh filter screen, (b) the relation between working distance and the corresponding nanofiber structure, image of the deposited area, and the resulting nanofiber diameter are incorporated (c & d) Images for the generated samples from conventional electrospinning and electro-blown spinning, respectively, and (e) The cone angle of the ejected solution jet from the electro-blown spinning setup [125].

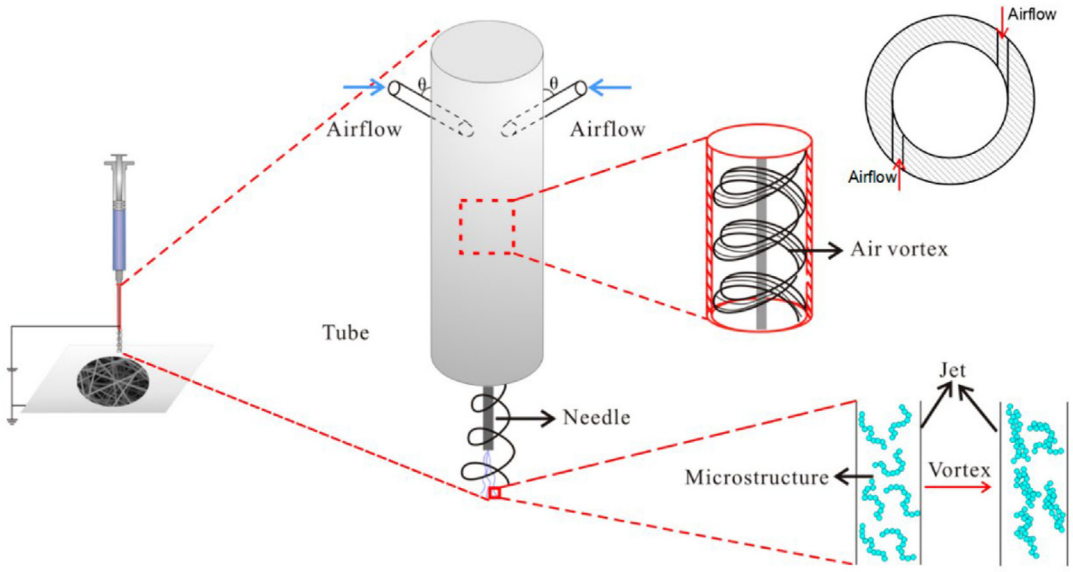

Fig. 13. Schematic drawing for the modified electrospinning air vortex setup [153].

structure to study the effect of air vortex forces on the PVA, and PAN membranes properties such as morphological characteristics, pore size, and mechanical strength [153]. The basic concept of the modified setup was to introduce a compressed airflow through two-opened holes around the solution ejection needle, which is housed inside a cylindrical tube. The airflow surrounds the solution jets causing an entanglement of the nanofiber chains. This change in the macromolecule chains due to vortex force showed a minimal effect on nanofiber diameter and membrane pore size. However, with increasing the airflow velocity from 0 to 4.5 m/s The maximum stress was noticeably increased from 5 to 8 MPa. The improvement in the mechanical strength can be attributed to the effect of the air vortex in generating entangled macromolecule chains which subsequently increase the possibility of nanofibers adhesion. So, extra forces are needed to overcome the friction.

6. Applications of electro-blown spinning nanofibers

The potential of the EBS process to conduct a wide range of materials and generate high-quality nanofibers mats has attracted

the researcher's interest for their implementation into several applications, see Fig. 14.

6.1. Filtration

Several studies have been recently introduced for the high capability of EBS membranes in water desalination and dye removal through DCMD process (Table 4). Styrene-acrylonitrile (SAN), acrylonitrile-butadiene-styrene (ABS), and polymethyl methacrylate (PMMA) with outstanding salt removal performance >99% were developed by Niknejad et al. via the EBS process [154–156]. For each material, the process parameters were optimized, and nanofiber diameter and membrane properties such as contact angle, mechanical durability, and water permeability were deeply examined. The EBS membranes exhibited a high permeate flux of (84.4 kg m^{-2} h^{-1}) and superior desalination capability for a wide range of saline water concentrations (35–250 g/L). Shirazi et al. synthesized a novel dual-layer EBS membrane structure from styrene-acrylonitrile (SAN) at the bottom and high-impact polystyrene (HIPS) at the top for industrial textile wastewater treatment by DCMD [157]. The results showed high robustness and noticeable contaminants removal up to 99.28%. However, a flux decline to 42.58% occurred after 48 h of filtration which can be ascribed to the effect of foulants accumulation onto the membrane surface. Niknejad et al. fabricated a SAN membrane for the removal of spent caustic from wastewater and compared the produced EBS mat with commercial polytetrafluoroethylene (PTFE) filter [158,159]. The SAN membranes exhibited a lower permeate flux owing to their higher thickness and surface hydrophobicity which hindered the intrusion of feed water through the membrane pores. Nevertheless, highly pure permeate with a stable flux of 12.03 kg/m^2. h and salt rejection of 99.98% was achieved during the 96 h distillation experiment. Khoshnevisan et al. studied the efficiency of superhydrophobic polystyrene (PS) membranes for dye wastewater treatment by DCMD through a wide range of synthetic dye concentrations (0.4, 0.8, and 1.2 g/L) to investigate their durability and fouling mechanism [160]. The proposed PS membrane appeared high dye removal factor of 99.8% for the different concentrations. However, the water permeability and membrane fouling were significantly increased by increasing the feed concentration due to the blockage of surface pores. Regarding the hydrophobic nature of the PS membrane, a stable surface water contact angle of > 90° was maintained during the DCMD experiments which makes it a suitable candidate for dying water treatment. Similarly, Li et al. introduced a facile construction of hierarchical porous alumina nanofibers via the simple PTFE emulsion template and EBS process for methylene-blue (MB) dye adsorption [161]. The authors demonstrated the effect of calcination temperature on the adsorption efficiency as well as porous structure. They found that with higher thermal treatment up to 800 °C, the surface area of the nanofibers mats noticeably increased to 226 m^2 g^{-1} which consequently increased the dye removal adsorption to 97% in 30 min. The superior dye removal capability of the alumina porous membrane originated from the surface and inner macro/mesoporous structures.

Different blending ratios of polystyrene (PS)/Polyacrylonitrile (PAN) nanofibers composite membranes were prepared by Fan et al. for oil/water separation [49]. Superior filtration capacity with permeate flux of 18,000 L m^{-2} h^{-1} that was retained for more than 10 filtration cycles was reported. In addition, the hydrophilic/oleophilic membrane exhibited oil/water separation >99% with an adequate mechanical strength of 5.8 MPa. Polylactic acid/polymethyl methacrylate (PLA/PMMA) transparent nanofibers mat was synthesized via the EBS process for airborne capture [170]. The fabricated membrane showed high transparency of 83% and superior filtration performance up to 99.5% for $PM_{2.5}$. The reason behind this remarkable filtration efficiency is the effect of the small surface pore size which is around 1.5 μm in hindering the particles from passing through the filter media. Hsiao et al. studied the relation between the membrane's mean flow pore size and air filtration characteristics of the polycarbonate nanofibers membrane [118]. A steady decrease in filtration efficiency was perceived with increasing the surface pore size due to the transport of aerosol particles within the flow. A similar trend resulted in pressure drop as the surface velocity increased with increasing the pore size, producing an observable reduction in pressure drop. Liu et al. proposed a free-standing Polyamide (PA-66) membrane via the EBS process to functionalize as a reusable personal protective mask [171]. They demonstrated a combined spinning technique based on the SBS and EBS processes (Fig. 15a and b) to generate scalable nanofibers mat with an average diameter of 61 nm. Moreover, a supplementary voltage supply assisted to separate the produced bundles into random-oriented nanofibers (Fig. 15c and d). As shown in Fig. 15e, $PM_{0.3}$ aerosol particulates were filtered through the PA-66 free-standing paper, and the conducted measurements showed a high filtration performance of 99% and a pressure drop of 125 Pa owing to the dominated mechanical particle-capture mechanism caused by the diameter of ultrasmall nanofibers.

The release of carcinogenic and toxic heavy metal ions from wastewater into the human body can pose a threat to both human health and the biological environment [172,173]. Paajanen et al. showed the performance of Tin oxide (SnO_2) and SnO_2/SiO_2 blend of EBS submicron nanofibers on the adsorption of cobalt II (Co^{2+}) ions [174]. Moreover, they studied the effect of nanofibers calcination at 400, 450, and 500 °C on the morphological and crystal structures of the produced membranes. All the pristine SnO_2 and SnO_2/SiO_2 composite mats exhibited a remarkable Co^{2+} uptake of more than 99% while the bare SnO_2 calcinated mat at 500 °C had

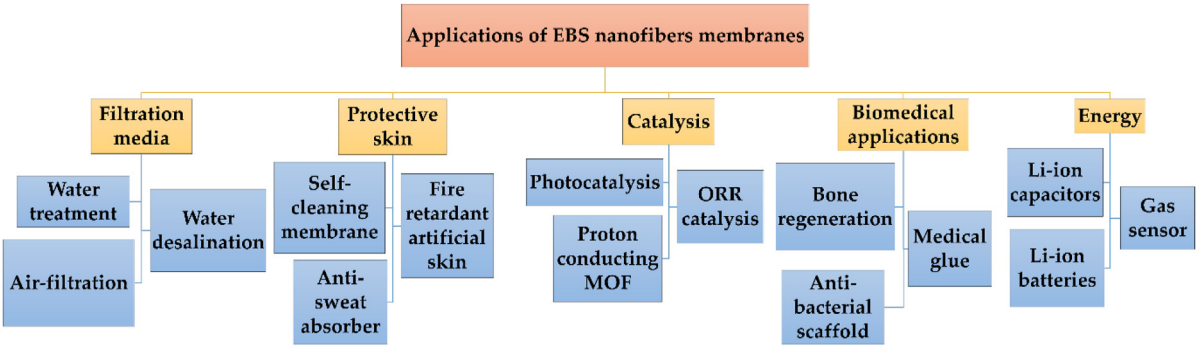

Fig. 14. Application of EBS nanofibers membranes.

Table 4
Properties and DCMD performance of the recently used EBS nanofibers membranes for water desalination.

Material	R (μm)	δ (μm)	ε (%)	WCA (°)	LEP (KPa)	J_W (kg/m^2.h)	t_P (hr)	R (%)	Ref.
Neat-SAN	3.68	845	96.2	145.7	40.8	10.24	14	98	[162]
HIPS	0.56	55	76	152.6	41	20.36	12	99.76	[163]
PS	0.41	116	75.5	160.4	160.4	48.1	24	99	[164]
Hot pressed- PS	0.562	65	74.7	154.52	38.6	22.5	6	99	[165]
SAN4-HIPS	0.43	180	77.8	121	135.6	23.56	48	99	[101]
PAN/SAN/PS	0.28	97.8	76.1	155.9	169.4	84.4	24	99	[166]
Hot pressed- SAN	0.18	105	70.3	133.4	118.9	41.8	24	99	[167]
PMMA	0.41	161	83.7	164.2	227.3	41	24	99	[168]
Hot pressed-ABS	0.24	123	72.3	157.8	185.1	54.3	24	99	[169]

Abbreviations: mean pore size, r; thickness, δ; porosity, ε; water contact angle, WCA; liquid entry pressure of water, LEP; permeate flux, J_w; DCMD duration, tp. Rejection factor, R.

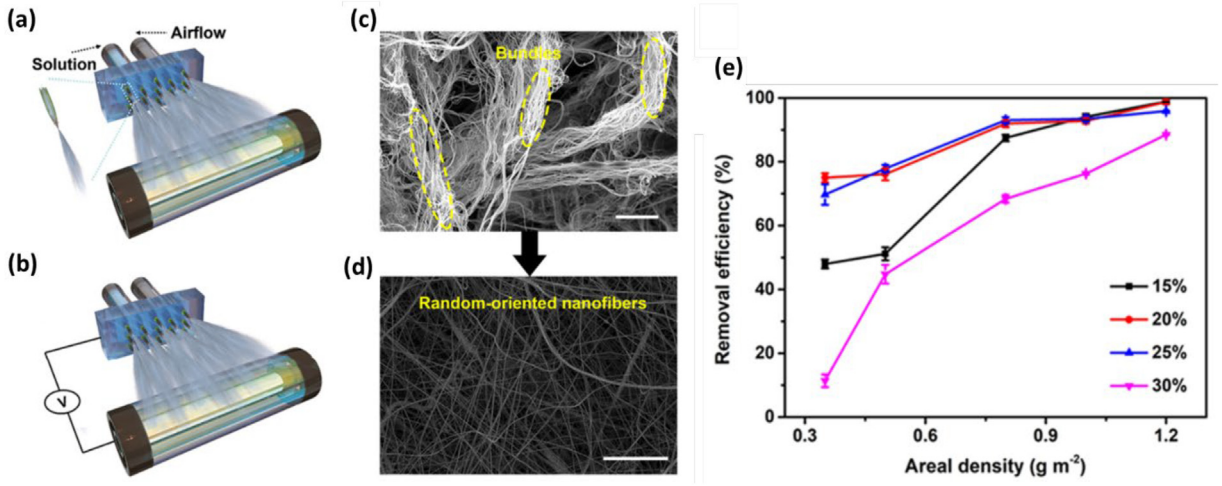

Fig. 15. (a) The conventional SBS multiple nozzle setup, (b) EBS setup with a connected electric field, the difference between the produced nanofibers (c) before and (d) after introducing the electric field, and (e) the relation between areal density & $PM_{0.3}$ removal efficiency for different PA-66 mass ratios membranes [171].

the highest adsorption coefficient because of its larger surface area compared to the other samples. Following the same procedure, Paajaan et al. also prepared a ZrO_2/PVP nanofibers membrane (Fig. 16a) for the removal of antimony Sb(V) from plant wastewater [175]. The same trend was confirmed for the calcinated zirconium mat at 500 °C after complete combustion of PVA (Fig. 16b), which showed the best potential for Sb(V) remediation with a maximum uptake of 8.6 mg. g^{-1} at pH 2, as shown in Fig. 16d. The authors also investigated the reusability of the Zirconium dioxide (ZrO_2) membrane by applying five consecutive adsorption cycles, as seen in Fig. 16c, the optimum sample of the calcinated membrane at 500 °C had the highest Sb(V) uptake of almost 6 mg/g for the first cycle before it then declines to 2.5 mg/g for the last one. The reason for that is the effect of calcination temperature on the crystal structure of ZrO_2 nanofibers. Luo et al. suggested that at this specific temperature of 500 °C, a tetragonal crystal structure of ZrO_2 is formed which is responsible for increasing the adsorption capacity along with its amount. However, below, or a further 500 °C, an amorphous and monoclinic phase can appear which causes a noticeable decline in the Sb(V) uptake [176].

Detecting another harmful heavy metal ion was conducted by Zhang et al. who demonstrated the adsorption affinity of the magnetic iron/ iron nitride (Fe/FeN_X) nanofibers to chromium (Cr (VI)) ions [177]. The influence of process parameters such as applied pressure, voltage, feeding rate, and calcination temperature on the resulting membrane properties was thoroughly investigated. The SEM images and surface area measurements detected a wide nanofiber diameter distribution in a range of 1–4 μm and a high specific surface area of 151 m^2 g^{-1} during thermal treatment at 800 °C. In addition, a relatively low removal efficiency for Cr (VI) ions with a maximum adsorption capacity of 79.21 mg/g was detected. Lonnrot et al. demonstrated the capability of Zirconium dioxide/antimony (ZrO_2/Sb) microfibers in the removal of pertechnetate (TcO_4−) by-products from wastewater [178]. Pertechnetate is an oxyanion structure that originates from uranium fusion in nuclear reactors. The composite microfibers attained high selectivity toward TcO_4 at a wide PH range f 1–10. Moreover, increasing the Sb concentration caused a slight increase in the membrane surface area from 49 to 54 m^2 g^{-1}.

6.2. Protective skin

A superhydrophobic self-cleaning membrane was prepared from SiO_2/PTFE EBS nanofibers to functionalize as a waterproof-breathable fabric [147]. The addition of SiO_2 significantly improved the membrane characteristics such as mechanical strength, hydrophobicity, and anti-corrosion behaviour. The modified non-woven mat exhibited a water contact angle of 153°. For durability and self-cleaning testing, the membrane was immersed in alkaline and acidic solutions for a long-time of up to 12 h. However, the self-cleaning membrane showed remarkable stable hydrophobicity and great potential for environmental self-cleaning applications.

Water-absorbing nanofibers scaffolds were synthesized from polyvinyl alcohol/chitosan (PVA/CS) for anti-sweat absorption [179]. Thermal treatment was implemented to attain hydrophilic

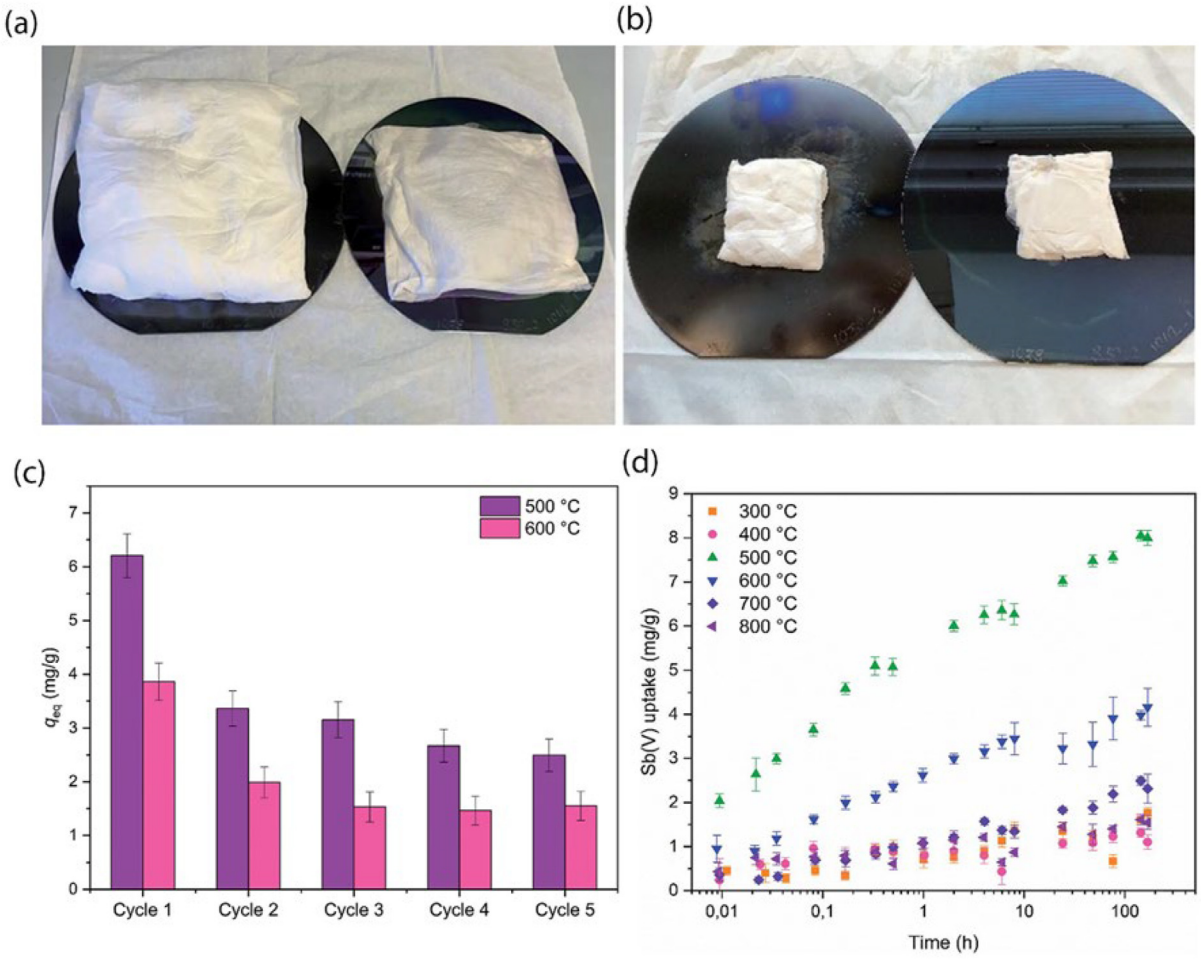

Fig. 16. (a) The EBS ZrO_2/PVP nanofibers membrane before calcination, (b) the pure ZrO2 membrane after calcination at 700 °C, (c) the reusability of optimized membranes through five successive cycles, and(d) the adsorption efficiency of the calcinated membranes for Sb(V) nanoparticles from 36 s to 100 h [175].

polymeric structure and enhance the swelling capability of the hybrid membrane. Results indicated fine and uniform nanofibers diameter of 80 nm and uttermost water absorption capacity >9000% at pH = 5 and normal temperature of 25 °C. Moreover, distilled water and artificial sweat were tested through the PVA/CS nanofibers membrane and a high swelling ratio of almost 7000% was observed for distilled water compared to artificial sweat which had a relatively lower absorption capacity of 1000%. Another research study was introduced by Aminyan et al. who demonstrated a superabsorbent PAA nanofibers hydrogel mat which had a nanofiber diameter of 312 nm and swilling ratios of 90,000% and 30,000% for distilled water and NaCl solution, respectively [180].

Smart composite nanofibers mat of silk nanoparticles incorporated into graphene sheets was recently developed and engineered to perform as a flame-retardant material and fire alarm system in artificial protective skins [50]. The multifunctional membrane sensor presented long-term stability, high porosity, and superior elasticity. The authors stated that the addition of graphene sheets significantly improved flame retardancy through the formation of a dense carbon layer on the top of the silk nanofibers layer, which in turn blocks the non-flammable gases from oxygen contact. The fire response is a significant concern in artificial skins as they are designed for use in a harsh flammable environment. Following that, the silk/graphene composite mat showed a rapid-fire alarm response of 2 s and superior fire resistance up to 300 s. Additionally, the silk/graphene nanofibers membrane can adhere to various substrates such as cellulose paper, PE non-woven substrate, and wood which verify its feasibility of implementation as a smart surface skin into robotic parts.

6.3. Catalysts

Continuous ultrafine nanofibers of CeO_2/CuO/Al_2O_3 blend were prepared and calcinated at 400 °C for photocatalytic activity applications [107]. The composite nanofibers were immersed in red solution acid at PH 6 under the effect of sunlight radiation. As shown in Fig. 17a, the higher surface area of the mat of 147 m^2g^{-1} predominately enhanced the dye degradation up to 90% by providing more active sites for dye absorption. Furthermore, the addition of Cu improved the catalytic activity up to 81% after 240 min of solar radiation emission in addition to increasing the durability and cyclability of the CeO_2/Al_2O_3 pristine membrane (Fig. 17b). This noticeable improvement is attributed to the lower energy band gap effect of CuO nanoparticles in facilitating the adsorption of sunlight and promoting the degradation process. A novel honeycomb-like carbon nanofibers (CNFs) structure was thermally treated in an air environment followed by second treatment processing in an N_2 atmosphere to fabricate an N–F-CNFs electrocatalyst electrode [181]. The unique characteristics of the co-doped mat such as large surface area, wide pore size distribution, and formation of high pyridine-N and graphite-N compounds, owed it an excellent oxygen-reduction reaction (ORR)

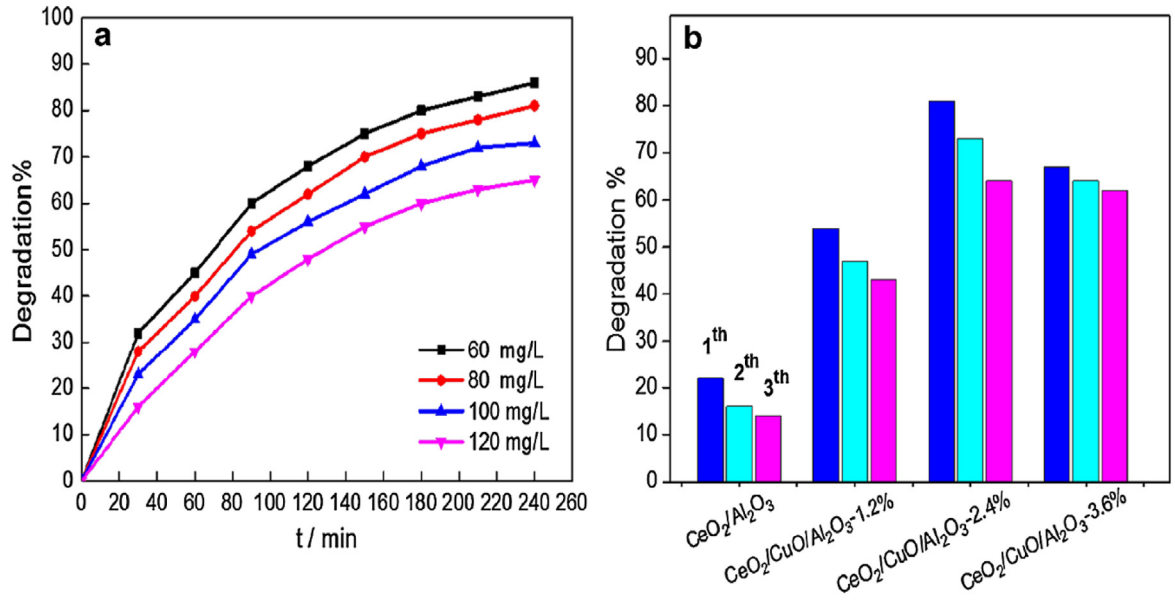

Fig. 17. (a) The degradation percentage for different concentrations of acid red dye through the $CeO_2/CuO/Al_2O_3$ NFs membrane, (b) the cyclability of CeO_2/Al_2O_3 & $CeO_2/CuO/Al_2O_3$ NFs membranes showing the effect of CuO content on improving the degradation performance [107].

potential of 0.606 V and 0.833 V in acidic and alkaline media, respectively.

Wang et al. synthesized a novel Al—NH_2 flower-like metal—organic framework (MOF) nanofibers which were incorporated into a sulfonated PES membrane matrix to generate a high-performance hybrid structure [131]. The MOF structure performed high tensile strength of 33.42 MPa and proton conductivity of 0.201 S cm^{-1}. The flower-like structure of the functionalized amino nanofibers retained a high surface area which operated as a proton pathway and strengthened the stability of the Al—NH_2 membrane. Moreover, the hydrophilic nature of the incorporated nanofibers rendered the hybrid membrane with sufficient water uptake up to 48%.

6.4. Biomedical

Implementing the EBS nanofibers scaffold in tissue engineering, cell culture, and bioactive applications has been broadly developed over the last few years. Mandakhbayar et al. demonstrated for the first time a cotton-like structure via the EBS process that was composed of bioactive glass nanoparticles (BGn) incorporated into polycaprolactone (PCL) nanofibers for bone engineering and defected bones regeneration [182]. The 3D fibrous mats were easily shaped and formed to fill defect spaces in addition to their capability to soak water and blood rapidly (Fig. 18a and b). Dental pulp-derived pluripotent stem cells effectively penetrated the scaffold network, anchored the nanofibers surface within hours, proliferated actively for weeks, and stimulated differentiation into osteogenic cells. As shown in Fig.18(c), the cell/scaffold construct was implanted into an extracted irregularly shaped alveolar bone defect to conform to the defect and stimulate early new bone formation.

Abdolbaghian et al. characterized the antibacterial activity of PLA/Sage nanofibers and core—shell hydrogel coaxial nanofibers mats [183]. Saga extract is one of the known plant species which owned a remarkable interest in medical applications including antibacterial, antifungal, antioxidants, etc. The importance of saga extract comes from its essential hydrophobic oils that can path through the stem cell walls, penetrating the cell membrane, and releasing metabolism which subsequently leads to the death of bacteria. The developed PLA/Sage EBS nanofibers showed a larger inhibition zone for gram-positive (*S. aureus*) and gram-negative (*E. coli*) bacteria with higher saga extract release compared to the core—shell system.

Medical glue of N-octyl-2-cyanoacrylate (OCA) and medical PMMA nanofibers were deposited into the wound surface using a homemade EBS setup to realize rapid hemostasis in dozens of seconds [184]. A low electric field of about 6—10 kV was conducted through a spinneret gun which assisted with airflow of 12 L/min. In vitro and in vivo hemostasis experiments were carried out on fresh pig livers. It was found that the EBS setup can generate a thick layer of OCA membrane onto the bleeding wound very precisely and rapidly just in 10 s. Moreover, the strength and compactness of the OCA membrane layer were tested by applying a force of 30 N, and strong adhesion of the nanofibers layer was resulted due to the self-assembled bonding between the OCA nanofibers layer and liver surface tissues.

6.5. Energy

Several recent studies have measured the efficiency of EBS nanofibers in lithium-ion batteries (LIB) [76,146,185—191]. PVDF nanofibers blended with modacrylic and SiO_2 nanoparticles were performed as a separator for LIB. The composite mat exhibited high porosity of 92%, electrolyte uptake of 606%, and ionic conductivity of 3.67 mS/cm [146]. Furthermore, the addition of SiO_2 nanoparticles has significantly enhanced the mechanical properties of the composite membrane due to the resulting crosslinking between the nanoparticles and polymer chains, while the modacrylic improved the flexibility and flame resistivity of the membrane. Another study proposed honeycomb porous carbon nanofibers doped with red phosphorus (P) nanoparticles as an anode for LIB [187]. The presented hybrid mat had a reversible capacity of 883 mAh g-1 after 100 cycles. The unique honeycomb structure of porous carbon was the main basis for its particular features by facilitating the movement of ions and electrons through the pores, increasing the membrane surface area, and protecting the active P from breaking which subsequently improved the access of electrolytes.

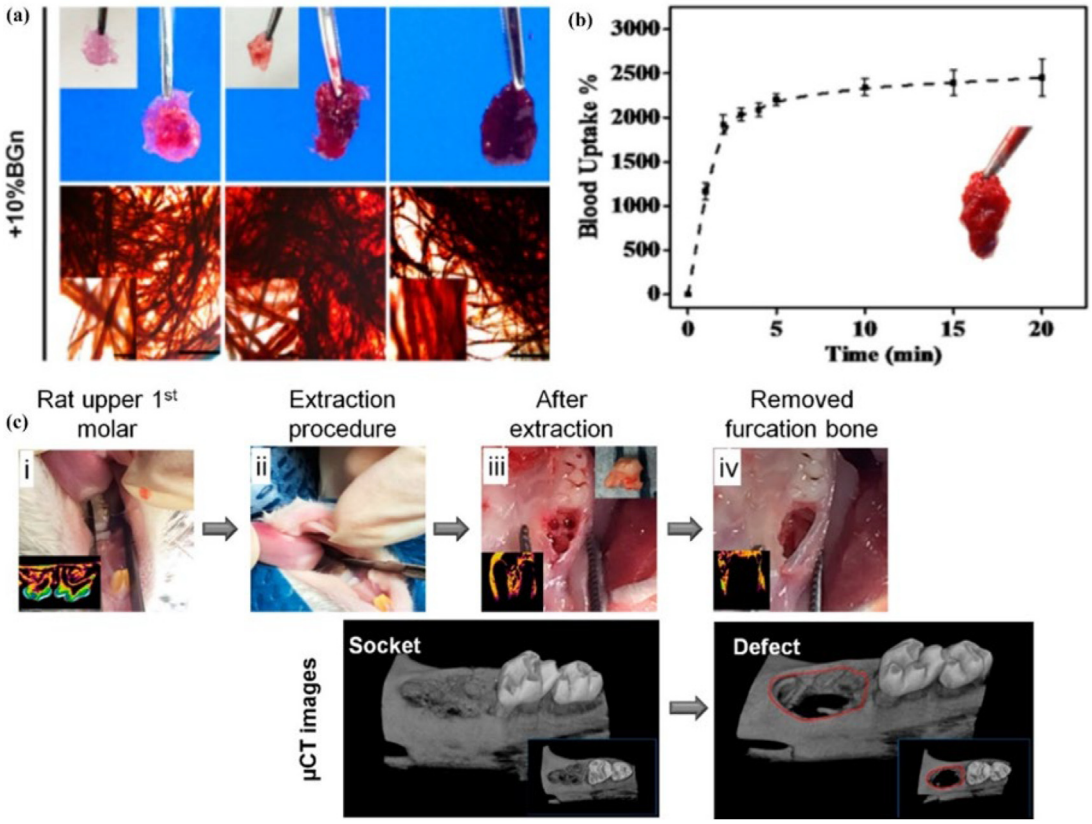

Fig. 18. (a) Optical images for the mineralization of cells examined by ARS assay for 10%BGn/PCL sample over three weeks (b) the blood uptake of the electro-blown cotton scaffold for 20 min, (c) In vivo modeling for the capacity of BGn/PCL scaffold to regenerate irregularly shaped defect in a rat alveolar (maxillary) bone for 8 weeks.

The performance of Manganese dioxide (MnO_2) nanosheets embedded into porous carbon nanofibers (CNFs) honeycomb structure was preliminarily examined for supercapacitor applications [192]. The prepared MnO_2/CNFs mat exhibited a discharge capacity of 421.5 F. g^{-1} at an applied current density of 0.5 A^{-1}. Furthermore, significantly cyclic stability of ~81% after 3000 cycles was observed due to the protection of MnO_2 nanosheets into the honeycomb cavity. PVA/PEDOT: PSS hybrid nanofibers membrane was prepared for sensing the ammonia gas in low concentrations [102]. Controlling the nanofiber diameter was achieved by increasing the applied voltage to 70 kV to investigate the effect of small diameter on the membrane surface area and the corresponding sensing performance. It was found that increasing the electric field from 20 to 70 kV can strongly decrease the nanofiber diameter from 263 nm to 68 nm. Furthermore, the response speed of the ultrafine nanofibers was much fast compared to thick

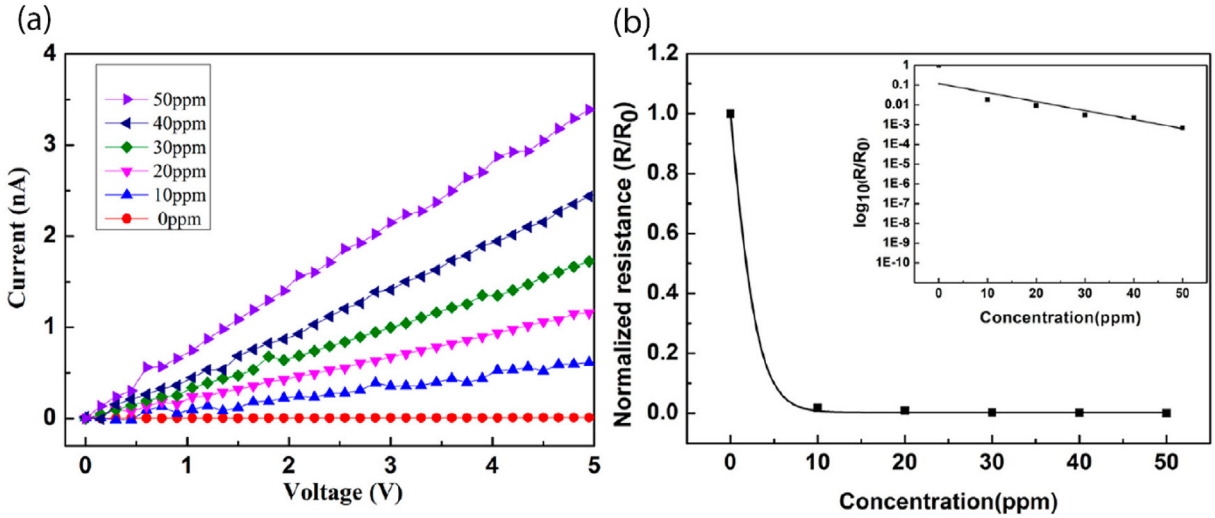

Fig. 19. (a) I–V curve, and (b) normalized resistance change for the ultrafine PVA/PEDOT: PSS nanofibers at different ammonia concentration [102].

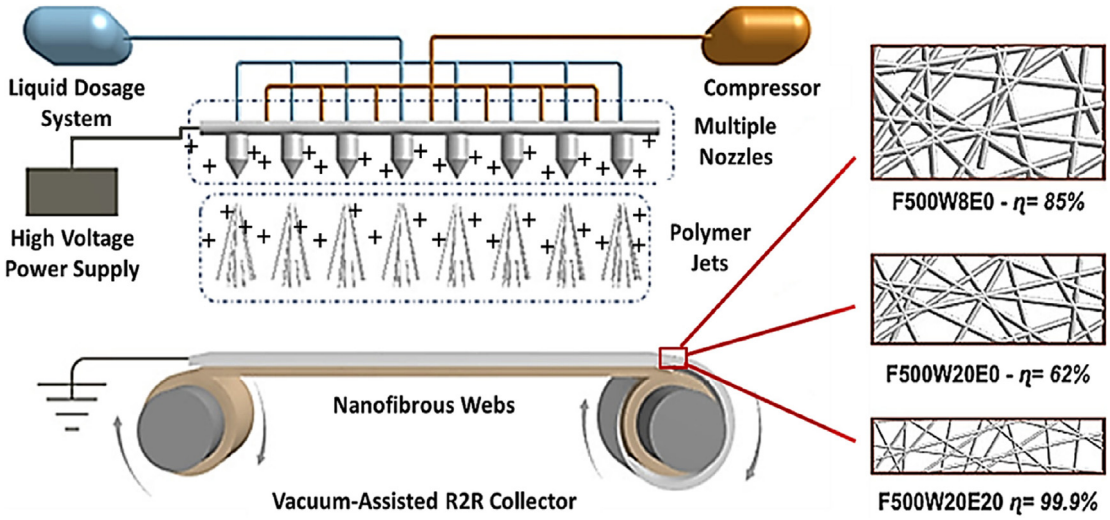

Fig. 20. EBS industrial scale system provided by AREKA company [148].

nanofibers at the same NH_3 concentration of 50 ppm (Fig. 19). This can be referred to the higher surface area of the ultrafine nanofibers membrane which provides more active sites for gas molecules.

7. Industrialization and challenges

According to the effect of electric field on enhancing the quality of EBS nanofibers and the capability of this integrated hybridized process in fabricating micro- and nano-large scale nanofibers scaffolds [193,194], many attempts have been made to show the potential of EBS for commercial applications. Industrial-scale EBS system was introduced by AREKA company which provided a multiple SBS nozzle holder that can inject each nozzle separately with polymer solution under an applied electric field as shown in Fig. 20 [148]. Polyamide (PA6) large-scale mat was fabricated for aerosol filtration and compared with the conventional SBS membrane performance. The results showed higher filtration efficiency for the EBS non-woven membrane of 99% while the SBS was around 85% associated with a pressure drop of 164 Pa. Moreover, the PA6 EBS membrane exhibited high solidity, smaller pore size, and long-term filtration stability. This superior capability of the PA6 membranes can be attributed to the effect of the electric field on

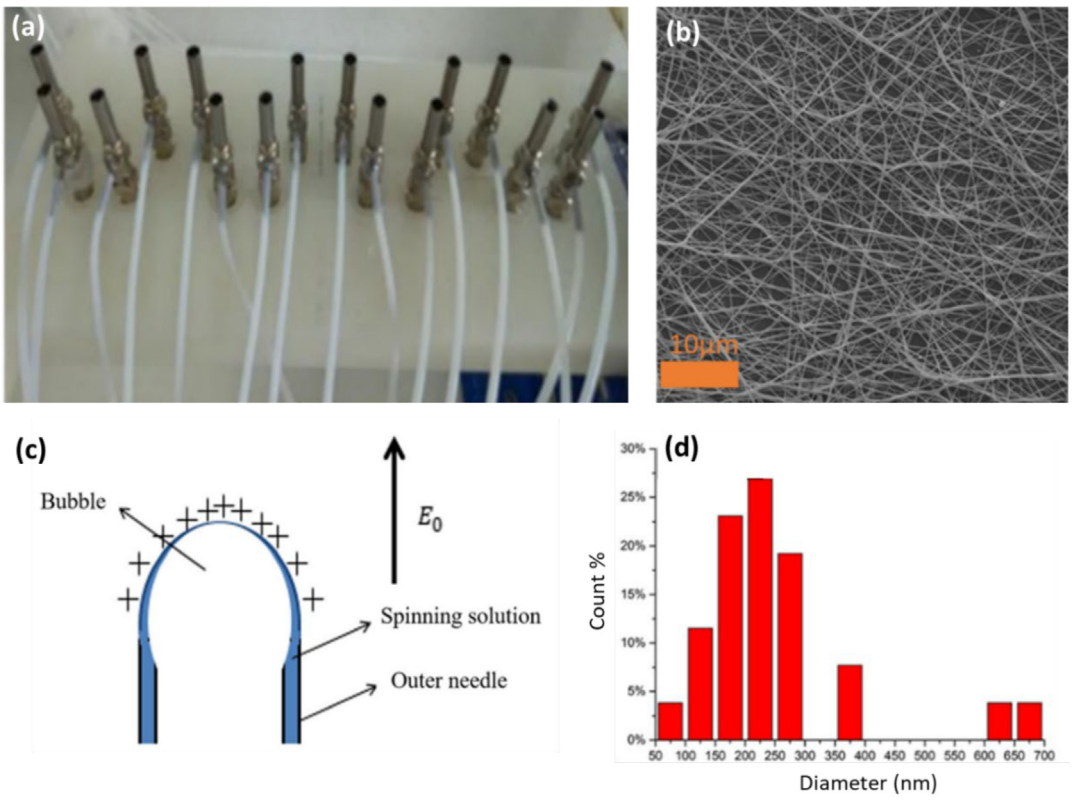

Fig. 21. (a) Multiple-nozzle EBS setup, (b) SEM image for the PVA nanofibers prepared at 45 kV, 0.1 MPa, 4 ml/h, and injection rate and 20 cm, (c) Schematic drawing for a charged bubble produced with pulsed gas, and (d) nanofibers diameter distribution of the optimized PVA nanofibers mat [195].

enhancing the spinning process and improving the quality of the nanofibers.

Gas-assisted multi-needle electrospinning setup was designed and manufactured for improving the productivity of conventional electrospinning [195]. Coaxial solution/gas auxiliary nozzle composed of an intermediate supplied gas shaft surrounded by an outer solution shaft was inserted into the EBS setup. The working principle of this innovative nozzle was based on inserting ruptured air bubbles into the polymer solution using pulsed airflow. Authors found that charging the bubbles with the aid of an electric field can significantly improve the spinning continuity and ejected jet distribution (Fig. 21c). Optimized process parameters were conducted through 16-pin multiple nozzle arrays (Fig. 21a) to produce an average nanofibers diameter of 200–250 nm (Fig. 21 (b & d)). Surprisingly, after half-hour of continuous spinning, uniform and thick nanofibers mat of 1.26 g which is 7.4 times of EBS single-nozzle, and 4.7 times of the air-free electrospinning was generated.

Multi-jet electrospinning and EBS were compared in fabricating PLLA nanofibers in terms of yield production, nanofibers diameter, and jet stability [196]. The SEM images and statistical analysis confirmed that the addition of airflow produced a membrane sample tenfold higher than conventional electrospinning, in addition to the smaller nanofiber diameter, jet stability, and controlled deposition. As mentioned earlier in Sec 2.3, the main advantage of combining the airflow and electric field is to overcome the repulsive forces between nanofibers which facilitate the formation of beads-free single oriented nanofibers instead of bundles.

There are still many challenges for the EBS process in the research stage. The key challenges for lab or industrial scale production can be concluded as follows (I) The safety hazard of electric field is considering a main challenge for EBS. Many research studies have already overcome the need for high voltage usage through various setup modifications. However, most of them are not suitable for the industrial scale production. (ii) Solvent recovery is a crucial challenge for the EBS process. The mass production of nanofibers via EBS will result in a lot of solvent consumption and volatilization. Which in sequence will increase the production costs and cause a major environmental problem. (iii) As the EBS process depends on both the airflow and electric field combined forces, minimum electrical conductivity needed to be provided in the polymer solution which limit the processible raw materials on the EBS.

8. Conclusion

Recently, EBS was introduced as a unique hybridization approach for producing high-quality and large-scale nanofiber mats. The EBS process is capable of producing uniform nanofiber diameters due to the effect of electric field and airflow merged driving forces. Those combined forces showed a remarkable improvement in the produced structure as well as solution jet stability. In this review paper, the working principle, reported materials, the influence of operating parameters on nanofiber diameter, and the implementation of EBS membranes into several applications are comprehensively reviewed. This review article also highlights the prospect of such new promising technology for fabricating a wide range of materials, including highly viscous polymers, as well as its potential for mass production and commercialization.

Declaration of competing interest

The authors declare that they have no known competing financial interests or personal relationships that could have appeared to influence the work reported in this paper

Acknowledgements

The authors would like to thank Edinburgh Napier University for providing a fully funded studentship as well as access to all facilities.

References

[1] A.B. Asha, R. Narain, Nanomaterials properties, in: Polymer Science and Nanotechnology, Elsevier, 2020, pp. 343–359, https://doi.org/10.1016/B978-0-12-816806-6.00015-7.
[2] P.N. Navya, H.K. Daima, Rational engineering of physicochemical properties of nanomaterials for biomedical applications with nanotoxicological perspectives, Nano Converg 3 (2016) 1, https://doi.org/10.1186/s40580-016-0064-z.
[3] B.S. Murty, P. Shankar, B. Raj, B.B. Rath, J. Murday, Unique properties of nanomaterials, in: Textbook of Nanoscience and Nanotechnology, Springer Berlin Heidelberg, Berlin, Heidelberg, 2013, pp. 29–65, https://doi.org/10.1007/978-3-642-28030-6_2.
[4] Q. Wu, W. Miao, Y. Zhang, H. Gao, D. Hui, Mechanical properties of nanomaterials: a review, Nanotechnol. Rev. 9 (2020) 259–273, https://doi.org/10.1515/ntrev-2020-0021.
[5] S.P. Patil, V.v. Burungale, Physical and chemical properties of nanomaterials, in: Nanomedicines for Breast Cancer Theranostics, Elsevier, 2020, pp. 17–31, https://doi.org/10.1016/B978-0-12-820016-2.00002-1.
[6] N. Chopra, V.G. Gavalas, L.G. Bachas, B.J. Hinds, L.G. Bachas, Functional one-dimensional nanomaterials: applications in nanoscale biosensors, Anal. Lett. 40 (2007) 2067–2096, https://doi.org/10.1080/00032710701567170.
[7] S.A. Mazari, E. Ali, R. Abro, F.S.A. Khan, I. Ahmed, M. Ahmed, et al., Nanomaterials: applications, waste-handling, environmental toxicities, and future challenges – a review, J. Environ. Chem. Eng. 9 (2021), 105028, https://doi.org/10.1016/j.jece.2021.105028.
[8] S. Das, B. Sen, N. Debnath, Recent trends in nanomaterials applications in environmental monitoring and remediation, Environ. Sci. Pollut. Control Ser. 22 (2015) 18333–18344, https://doi.org/10.1007/s11356-015-5491-6.
[9] A.S. Edelstein, R.C. Cammaratra (Eds.), Nanomaterials, CRC Press, 1998, https://doi.org/10.1201/9781482268591.
[10] T.A. Saleh, Nanomaterials: classification, properties, and environmental toxicities, Environ. Technol. Innov. 20 (2020), 101067, https://doi.org/10.1016/j.eti.2020.101067.
[11] N. Abid, A.M. Khan, S. Shujait, K. Chaudhary, M. Ikram, M. Imran, et al., Synthesis of nanomaterials using various top-down and bottom-up approaches, influencing factors, advantages, and disadvantages: a review, Adv. Colloid Interface Sci. 300 (2022), 102597, https://doi.org/10.1016/j.cis.2021.102597.
[12] V. Singh, P. Yadav, V. Mishra, Recent advances on classification, properties, synthesis, and characterization of nanomaterials, in: Green Synthesis of Nanomaterials for Bioenergy Applications, Wiley, 2020, pp. 83–97, https://doi.org/10.1002/9781119576785.ch3.
[13] L. Wei, X. Qin, Nanofiber bundles and nanofiber yarn device and their mechanical properties: a review, Textil. Res. J. 86 (2016) 1885–1898, https://doi.org/10.1177/0040517515617422.
[14] C.T. Kenry, Lim, Nanofiber technology: current status and emerging developments, Prog. Polym. Sci. 70 (2017) 1–17, https://doi.org/10.1016/j.progpolymsci.2017.03.002.
[15] Z.-M. Huang, Y.-Z. Zhang, M. Kotaki, S. Ramakrishna, A review on polymer nanofibers by electrospinning and their applications in nanocomposites, Compos. Sci. Technol. 63 (2003) 2223–2253, https://doi.org/10.1016/S0266-3538(03)00178-7.
[16] J. Xue, J. Xie, W. Liu, Y. Xia, Electrospun Nanofibers: New Concepts, Materials, and Applications, 2017, https://doi.org/10.1021/acs.accounts.7b00218.
[17] S. Thenmozhi, N. Dharmaraj, K. Kadirvelu, H.Y. Kim, Electrospun nanofibers: new generation materials for advanced applications, Mater. Sci. Eng., B 217 (2017) 36–48, https://doi.org/10.1016/j.mseb.2017.01.001.
[18] R.L. Dahlin, F.K. Kasper, A.G. Mikos, Polymeric nanofibers in tissue engineering, Tissue Eng. B Rev. 17 (2011) 349–364, https://doi.org/10.1089/ten.teb.2011.0238.
[19] A. Ghajarieh, S. Habibi, A. Talebian, Biomedical applications of nanofibers, Russ. J. Appl. Chem. 94 (2021) 847–872, https://doi.org/10.1134/S1070427221070016.
[20] I. Alghoraibi, S. Alomari, Different methods for nanofiber design and fabrication, in: Handbook of Nanofibers, Springer International Publishing, Cham, 2018, pp. 1–46, https://doi.org/10.1007/978-3-319-42789-8_11-2.
[21] T. Garg, G. Rath, A.K. Goyal, Biomaterials-based nanofiber scaffold: targeted and controlled carrier for cell and drug delivery, J. Drug Target. 23 (2015) 202–221, https://doi.org/10.3109/1061186X.2014.992899.
[22] J. Xue, T. Wu, Y. Dai, Y. Xia, Electrospinning and Electrospun Nanofibers: Methods, Materials, and Applications, 2019, https://doi.org/10.1021/acs.chemrev.8b00593.
[23] J. Yan, Y. Han, S. Xia, X. Wang, Y. Zhang, J. Yu, et al., Polymer Template Synthesis of Flexible BaTiO 3 Crystal Nanofibers, 2019, https://doi.org/10.1002/adfm.201907919.

[24] S.I. Park, H.-M. Song, Bottom-up self-assembly of nanofibers in the surfactant mixture of CTAB and Pluronics ARTICLES YOU MAY BE INTERESTED IN Bottom-up self-assembly of nanofibers in the surfactant mixture of CTAB and Pluronics, AIP Adv. 11 (2021), 125031, https://doi.org/10.1063/5.0077041.
[25] F. Zuo, D.H. Tan, Z. Wang, S. Jeung, C.W. Macosko, F.S. Bates, Nanofibers from melt blown fiber-in-fiber, Polymer Blends 14 (2013) 2, https://doi.org/10.1021/mz400053n.
[26] X. Zhang, Y. Lu, Polymer reviews centrifugal spinning: an alternative approach to fabricate nanofibers at high speed and low cost centrifugal spinning: an alternative approach to fabricate nanofibers at high speed and low cost, Polym. Rev. 54 (2014) 677–701, https://doi.org/10.1080/15583724.2014.935858.
[27] J. Song, M. Kim, H. Lee, polymers Recent Advances on Nanofiber Fabrications: Unconventional State-of-the-Art Spinning Techniques, (n.d.). https://doi.org/10.3390/polym12061386.
[28] F. Liu, S. Li, Y. Fang, F. Zheng, J. Li, J. He, Fabrication of highly oriented nanoporous fibers via airflow bubble-spinning, Appl. Surf. Sci. 421 (2017) 61–67, https://doi.org/10.1016/j.apsusc.2017.01.204.
[29] Y. Fang, F. Liu, L. Xu, P. Wang, J. He, Preparation of PLGA/MWCNT composite nanofibers by airflow bubble-spinning and their characterization, Polymers 10 (2018) 481, https://doi.org/10.3390/polym10050481.
[30] X. Hu, X. Zhang, Xiaodong Shen, H. Li, Osamu Takai, N. Saito, et al., Plasma-induced synthesis of CuO nanofibers and ZnO nanoflowers in water, Plasma Chem. Plasma Process. 34 (2014) 1129–1139, https://doi.org/10.1007/s11090-014-9546-0.
[31] A. Suzuki, T. Mikuni, T. Hasegawa, Nylon 66 nanofibers prepared by CO 2 laser supersonic drawing, J. Appl. Polym. Sci. (2013), 40015, https://doi.org/10.1002/app.40015.
[32] Y. Huang, N. Bu, Y. Duan, Y. Pan, H. Liu, Z. Yin, et al., Electrohydrodynamic direct-writing, Nanoscale 5 (2013), 12007, https://doi.org/10.1039/c3nr04329k.
[33] E.S. Medeiros, G.M. Glenn, A.P. Klamczynski, W.J. Orts, L.H.C. Mattoso, Solution blow spinning: a new method to produce micro-and nanofibers from polymer solutions, J. Appl. Polym. Sci. 113 (2009) 2322–2330, https://doi.org/10.1002/app.30275.
[34] L. Wang, Functional nanofibre: enabling material for the next generation smart textiles, J. Fiber Bioeng. Inf. 1 (2008) 81–92, https://doi.org/10.3993/jfbi09200801.
[35] A. Mamun, T. Blachowicz, L. Sabantina, Polymers Electrospun Nanofiber Mats for Filtering Applications-Technology, Structure and Materials, 2021, https://doi.org/10.3390/polym13091368.
[36] R. Rasouli, A. Barhoum, M. Bechelany, A.R. Dufresne Rasouli, A. Barhoum, M. Bechelany, et al., REVIEW 1800256 (1 of 27) Nanofibers for Biomedical and Healthcare Applications, 2018, https://doi.org/10.1002/mabi.201800256.
[37] N. Shehata, E. Elnabawy, M. Abdelkader, A.H. Hassanin, M. Salah, R. Nair, et al., Static-Aligned Piezoelectric Poly (Vinylidene Fluoride) Electrospun Nanofibers/MWCNT Composite Membrane: Facile Method, (n.d.). https://doi.org/10.3390/polym10090965.
[38] N. Shehata, R. Nair, R. Boualayan, I. Kandas, A. Masrani, E. Elnabawy, et al., Stretchable nanofibers of polyvinylidenefluoride (PVDF)/thermoplastic polyurethane (TPU) nanocomposite to support piezoelectric response via mechanical elasticity, (123AD). https://doi.org/10.1038/s41598-022-11465-5.
[39] E. Elnabawy, M. Farag, A. Soliman, K. Mahmoud, N. Shehata, R. Nair, et al., Solution blow spinning of piezoelectric nanofiber mat for detecting mechanical and acoustic signals, J. Appl. Polym. Sci. 138 (2021), https://doi.org/10.1002/app.51322.
[40] F. Yilmaz, G. Celep, G. Tetik, Nanofibers in cosmetics, in: Nanofiber Research - Reaching New Heights, InTech, 2016, https://doi.org/10.5772/64172.
[41] A.H. Nurfaizey, N. Tucker, J. Stanger, M.P. Staiger, Functional nanofibers in clothing for protection against chemical and biological hazards, in: Functional Nanofibers and Their Applications, Elsevier, 2012, pp. 236–261, https://doi.org/10.1533/9780857095640.2.236.
[42] M. Pardo-Figuerez, A. Chiva-Flor, K. Figueroa-Lopez, C. Prieto, J.M. Lagaron, Antimicrobial Nanofiber Based Filters for High Filtration Efficiency Respirators, 2021, https://doi.org/10.3390/nano.
[43] Z. Li, Z. Cui, L. Zhao, N. Hussain, Y. Zhao, C. Yang, et al., High-throughput production of kilogram-scale nanofibers by Kármán vortex solution blow spinning, Sci. Adv. 8 (2022), https://doi.org/10.1126/sciadv.abn3690.
[44] S. Omer, L. Forgách, R. Zelkó, I. Sebe, Pharmaceutics Scale-Up of Electrospinning: Market Overview of Products and Devices for Pharmaceutical and Biomedical Purposes, 2021, https://doi.org/10.3390/pharmaceutics13020286.
[45] L. Wang, Y. Gao, J. Xiong, W. Shao, C. Cui, N. Sun, et al., Biodegradable and high-performance multiscale structured nanofiber membrane as mask filter media via poly(lactic acid) electrospinning, J. Colloid Interface Sci. 606 (2022) 961–970, https://doi.org/10.1016/j.jcis.2021.08.079.
[46] Smart composite nanofiber mats with thermal management functionality Nuray Kizildag, (n.d.). https://doi.org/10.1038/s41598-021-83799-5.
[47] I. Alghoraibi, S. Alomari, Different methods for nanofiber design and fabrication, in: Handbook of Nanofibers, Springer International Publishing, Cham, 2018, pp. 1–46, https://doi.org/10.1007/978-3-319-42789-8_11-2.
[48] J. Ju, W. Kang, L. Li, H. He, C. Qiao, B. Cheng, Preparation of poly (tetrafluoroethylene) nanofiber film by electro-blown spinning method, Mater. Lett. 171 (2016) 236–239, https://doi.org/10.1016/j.matlet.2016.02.089.
[49] L. Fan, J. Yan, H. He, N. Deng, Y. Zhao, W. Kang, et al., Electro-blown spun PS/PAN fibrous membrane for highly efficient oil/water separation, Fibers Polym. 18 (2017) 1988–1994, https://doi.org/10.1007/s12221-017-7429-8.
[50] L. Cao, Q. Liu, J. Ren, W. Chen, Y. Pei, D.L. Kaplan, et al., Electro-blown spun silk/graphene nanoionotronic skin for multifunctional fire protection and alarm, Adv. Mater. 33 (2021), https://doi.org/10.1002/adma.202102500.
[51] Y. Liu, J. Wen, B. Chen, M. Zheng, D. Liu, Y. Liu, et al., Electro-blown spinning driven by cylindrical rotating triboelectric nanogenerator and its applications for fabricating nanofibers, Appl. Mater. Today 19 (2020), https://doi.org/10.1016/j.apmt.2020.100631.
[52] L. Li, W. Kang, X. Zhuang, J. Shi, Y. Zhao, B. Cheng, A comparative study of alumina fibers prepared by electro-blown spinning (EBS) and solution blowing spinning (SBS), Mater. Lett. 160 (2015) 533–536, https://doi.org/10.1016/j.matlet.2015.08.016.
[53] J. Ju, W. Kang, N. Deng, L. Li, Y. Zhao, X. Ma, et al., Preparation and characterization of PVA-based carbon nanofibers with honeycomb-like porous structure via electro-blown spinning method, Microporous Mesoporous Mater. 239 (2017) 416–425, https://doi.org/10.1016/j.micromeso.2016.10.024.
[54] I.C. Um, D. Fang, B.S. Hsiao, A. Okamoto, B. Chu, Electro-spinning and electro-blowing of hyaluronic acid, Biomacromolecules 5 (2004) 1428–1436, https://doi.org/10.1021/bm034539b.
[55] G. Xu, X. Chen, Z. Zhu, P. Wu, H. Wang, X. Chen, et al., Pulse gas-assisted multi-needle electrospinning of nanofibers, Adv. Compos. Hybrid Mater. 3 (2020) 98–113, https://doi.org/10.1007/s42114-019-00129-0.
[56] W. Zheng, W. Zheng, C. Shi, X. Wang, Cylindrical-electrode-assisted solution blowing for nanofiber spinning, J. Appl. Polym. Sci. 136 (2019), https://doi.org/10.1002/app.47087.
[57] D. Tang, X. Zhuang, C. Zhang, B. Cheng, X. Li, Generation of nanofibers via electrostatic-Induction-assisted solution blow spinning, J. Appl. Polym. Sci. 132 (2015), https://doi.org/10.1002/app.42326.
[58] I. Alghoraibi, S. Alomari, Different methods for nanofiber design and fabrication, in: Handbook of Nanofibers, Springer International Publishing, Cham, 2018, pp. 1–46, https://doi.org/10.1007/978-3-319-42789-8_11-2.
[59] J. Xue, T. Wu, Y. Dai, Y. Xia, Electrospinning and electrospun nanofibers: methods, materials, and applications, Chem. Rev. 119 (2019) 5298–5415, https://doi.org/10.1021/acs.chemrev.8b00593.
[60] C. Chen, M. Dirican, X. Zhang, Centrifugal spinning—high rate production of nanofibers, in: Electrospinning: Nanofabrication and Applications, Elsevier, 2019, pp. 321–338, https://doi.org/10.1016/B978-0-323-51270-1.00010-8.
[61] J.L. Daristotle, A.M. Behrens, A.D. Sandler, P. Kofinas, A review of the fundamental principles and applications of solution blow spinning, ACS Appl. Mater. Interfaces 8 (2016) 34951–34963, https://doi.org/10.1021/acsami.6b12994.
[62] C.J. Ellison, A. Phatak, D.W. Giles, C.W. Macosko, F.S. Bates, Melt blown nanofibers: fiber diameter distributions and onset of fiber breakup, Polymer 48 (2007) 3306–3316, https://doi.org/10.1016/j.polymer.2007.04.005.
[63] A.N. Moore, J.D. Hartgerink, Self-assembling multidomain peptide nanofibers for delivery of bioactive molecules and tissue regeneration, Acc. Chem. Res. 50 (2017) 714–722, https://doi.org/10.1021/acs.accounts.6b00553.
[64] M. Wojasiński, M. Pilarek, T. Ciach, Comparative studies of electrospinning and solution blow spinning processes for the production of nanofibrous poly(L-lactic acid) materials for biomedical engineering, Pol. J. Chem. Technol. 16 (2014) 43–50, https://doi.org/10.2478/pjct-2014-0028.
[65] J. Ahmed, R.K. Matharu, T. Shams, U.E. Illangakoon, M. Edirisinghe, A comparison of electric-field-driven and pressure-driven fiber generation methods for drug delivery, Macromol. Mater. Eng. 303 (2018), 1700577, https://doi.org/10.1002/mame.201700577.
[66] I.C. Um, D. Fang, B.S. Hsiao, A. Okamoto, B. Chu, Electro-spinning and electro-blowing of hyaluronic acid, Biomacromolecules 5 (2004) 1428–1436, https://doi.org/10.1021/bm034539b.
[67] X. Wang, I.C. Um, D. Fang, A. Okamoto, B.S. Hsiao, B. Chu, Formation of water-resistant hyaluronic acid nanofibers by blowing-assisted electro-spinning and non-toxic post treatments, Polymer 46 (2005) 4853–4867, https://doi.org/10.1016/j.polymer.2005.03.058.
[68] X. Wang, I.C. Um, D. Fang, A. Okamoto, B.S. Hsiao, B. Chu, Formation of water-resistant hyaluronic acid nanofibers by blowing-assisted electro-spinning and non-toxic post treatments, Polymer 46 (2005) 4853–4867, https://doi.org/10.1016/j.polymer.2005.03.058.
[69] Y. Lin, Y. Yao, X. Yang, L. Shen, R. Li, D. Wu, Effect of gas flow rate on crystal structures of electrospun and gas-jet/electrospun poly(vinylidene fluoride) fibers, Chin. J. Polym. Sci. 27 (2009) 511, https://doi.org/10.1142/S0256767909004187.
[70] N. Bhardwaj, S.C. Kundu, Electrospinning: a fascinating fiber fabrication technique, Biotechnol. Adv. 28 (2010) 325–347, https://doi.org/10.1016/j.biotechadv.2010.01.004.
[71] J.-H. He, On the height of Taylor cone in electrospinning, Results Phys. 17 (2020), 103096, https://doi.org/10.1016/j.rinp.2020.103096.
[72] R. Scaffaro, M. Gammino, A. Maio, Wet electrospinning-aided self-assembly of multifunctional GO-CNT@PCL core-shell nanocomposites with spider leg bioinspired hierarchical architectures, Compos. Sci. Technol. 221 (2022), 109363, https://doi.org/10.1016/j.compscitech.2022.109363.
[73] J. Yin, A. Ahmed, L. Xu, High-throughput free surface electrospinning using solution reservoirs with different depths and its preparation mechanism

study, Advanced Fiber Materials 3 (2021) 251–264, https://doi.org/10.1007/s42765-021-00078-8.
[74] Y. Liu, X. Zhang, Y. Xia, H. Yang, Magnetic-field-assisted electrospinning of aligned straight and wavy polymeric nanofibers, Adv. Mater. 22 (2010) 2454–2457, https://doi.org/10.1002/adma.200903870.
[75] J. Kerwald, C.F. de Moura Junior, E.D. Freitas, J.D.P. de Moraes Segundo, R.S. Vieira, M.M. Beppu, Cellulose-based electrospun nanofibers: a review, Cellulose 29 (2022) 25–54, https://doi.org/10.1007/s10570-021-04303-w.
[76] C. Ye, L. Xu, Heteroatom-doped porous carbon derived from zeolite imidazole framework/polymer core-shell fibers as an electrode material for supercapacitor, Compos. B Eng. 225 (2021), 109256, https://doi.org/10.1016/j.compositesb.2021.109256.
[77] K. Havlíček, L. Svobodová, T. Bakalova, T. Lederer, Influence of electrospinning methods on characteristics of polyvinyl butyral and polyurethane nanofibres essential for biological applications, Mater. Des. 194 (2020), 108898, https://doi.org/10.1016/j.matdes.2020.108898.
[78] J. Hong, M. Yeo, G.H. Yang, G. Kim, Cell-electrospinning and its application for tissue engineering, Int. J. Mol. Sci. 20 (2019) 6208, https://doi.org/10.3390/ijms20246208.
[79] J. Yin, L. Xu, A. Ahmed, Batch preparation and characterization of electrospun porous polylactic acid-based nanofiber membranes for antibacterial wound dressing, Advanced Fiber Materials 4 (2022) 832–844, https://doi.org/10.1007/s42765-022-00141-y.
[80] S. Yu, Y. Tai, J. Milam-Guerrero, J. Nam, N.v. Myung, Electrospun organic piezoelectric nanofibers and their energy and bio applications, Nano Energy 97 (2022), 107174, https://doi.org/10.1016/j.nanoen.2022.107174.
[81] X. Qin, S. Subianto, Electrospun nanofibers for filtration applications, in: Electrospun Nanofibers, Elsevier, 2017, pp. 449–466, https://doi.org/10.1016/B978-0-08-100907-9.00017-9.
[82] N. Yin, F. Liu, Nanofibrous filters for PM2.5 filtration: conception, mechanism and progress, Nano 16 (2021), 2130004, https://doi.org/10.1142/S1793292021300048.
[83] S. Pongampai, T. Charoonsuk, N. Pinpru, P. Pulphol, W. Vittayakorn, P. Pakawanit, et al., Triboelectric-piezoelectric hybrid nanogenerator based on BaTiO3-Nanorods/Chitosan enhanced output performance with self-charge-pumping system, Compos. B Eng. 208 (2021), 108602, https://doi.org/10.1016/j.compositesb.2020.108602.
[84] M. Kumar, P. kumari, P. sahatiya, P(VDF-TrFE)/ZnO nanofiber composite based piezoelectric nanogenerator as self-powered sensor: fabrication and characterization, J. Polym. Res. 29 (2022) 44, https://doi.org/10.1007/s10965-022-02890-1.
[85] W. Chen, W. Fan, Q. Wang, X. Yu, Y. Luo, W. Wang, et al., A nano-micro structure engendered abrasion resistant, superhydrophobic, wearable triboelectric yarn for self-powered sensing, Nano Energy 103 (2022), 107769, https://doi.org/10.1016/j.nanoen.2022.107769.
[86] J. Kang, T. Liu, Y. Lu, L. Lu, K. Dong, S. Wang, et al., Polyvinylidene fluoride piezoelectric yarn for real-time damage monitoring of advanced 3D textile composites, Compos. B Eng. 245 (2022), 110229, https://doi.org/10.1016/j.compositesb.2022.110229.
[87] L. Xue, W. Fan, Y. Yu, K. Dong, C. Liu, Y. Sun, et al., A novel strategy to fabricate core-sheath structure piezoelectric yarns for wearable energy harvesters, Advanced Fiber Materials 3 (2021) 239–250, https://doi.org/10.1007/s42765-021-00081-z.
[88] T.T. Le, E.J. Curry, T. Vinikoor, R. Das, Y. Liu, D. Sheets, et al., Piezoelectric nanofiber membrane for reusable, stable, and highly functional face mask filter with long-term biodegradability, Adv. Funct. Mater. 32 (2022), 2113040, https://doi.org/10.1002/adfm.202113040.
[89] J. Hong, M. Yeo, G.H. Yang, G. Kim, Cell-electrospinning and its application for tissue engineering, Int. J. Mol. Sci. 20 (2019) 6208, https://doi.org/10.3390/ijms20246208.
[90] J. Nam, Y. Huang, S. Agarwal, J. Lannutti, Materials selection and residual solvent retention in biodegradable electrospun fibers, J. Appl. Polym. Sci. 107 (2008) 1547–1554, https://doi.org/10.1002/app.27063.
[91] Y. Gao, J. Zhang, Y. Su, H. Wang, X.-X. Wang, L.-P. Huang, et al., Recent progress and challenges in solution blow spinning, Mater. Horiz. 8 (2021) 426–446, https://doi.org/10.1039/D0MH01096K.
[92] E.S. Medeiros, G.M. Glenn, A.P. Klamczynski, W.J. Orts, L.H.C. Mattoso, Solution blow spinning: a new method to produce micro- and nanofibers from polymer solutions, J. Appl. Polym. Sci. 113 (2009) 2322–2330, https://doi.org/10.1002/app.30275.
[93] J.L. Daristotle, A.M. Behrens, A.D. Sandler, P. Kofinas, A review of the fundamental principles and applications of solution blow spinning, ACS Appl. Mater. Interfaces 8 (2016) 34951–34963, https://doi.org/10.1021/acsami.6b12994.
[94] M. Wojasiński, T. Ciach, Production of Polymer Fibres by Solution Blow Spinning Conference Paper April 2013 CITATIONS 2 READS 970 BioGraft-Biomimetic Prosthesis of Small Diameter View Project BioCoatGraft: Small Diameter Vascular Prostheses with Bioactive Coating: Analysis of Hemocompatibility and Endothelial Cell Response View Project, n.d, https://www.researchgate.net/publication/255485277.
[95] R. Atif, J. Khaliq, M. Combrinck, A.H. Hassanin, N. Shehata, E. Elnabawy, et al., Solution blow spinning of polyvinylidene fluoride based fibers for energy harvesting applications: a review, Polymers 12 (2020) 1304, https://doi.org/10.3390/polym12061304.
[96] S. Sinha-Ray, A.L. Yarin, B. Pourdeyhimi, The production of 100/400nm inner/outer diameter carbon tubes by solution blowing and carbonization of core–shell nanofibers, Carbon N Y 48 (2010) 3575–3578, https://doi.org/10.1016/j.carbon.2010.05.056.
[97] A. Kolbasov, S. Sinha-Ray, A. Joijode, M.A. Hassan, D. Brown, B. Maze, et al., Industrial-scale solution blowing of soy protein nanofibers, Ind. Eng. Chem. Res. 55 (2016) 323–333, https://doi.org/10.1021/acs.iecr.5b04277.
[98] W. Han, S. Xie, X. Sun, X. Wang, Z. Yan, Optimization of airflow field via solution blowing for chitosan/PEO nanofiber formation, Fibers Polym. 18 (2017) 1554–1560, https://doi.org/10.1007/s12221-017-7213-9.
[99] R. Atif, M. Combrinck, J. Khaliq, A.H. Hassanin, N. Shehata, E. Elnabawy, et al., Solution blow spinning of high-performance submicron polyvinylidene fluoride fibres: computational fluid mechanics modelling and experimental results, Polymers 12 (2020) 1140, https://doi.org/10.3390/polym12051140.
[100] E. Elnabawy, M. Farag, A. Soliman, K. Mahmoud, N. Shehata, R. Nair, et al., Solution blow spinning of piezoelectric nanofiber mat for detecting mechanical and acoustic signals, J. Appl. Polym. Sci. 138 (2021), 51322, https://doi.org/10.1002/app.51322.
[101] M.M.A. Shirazi, S. Bazgir, F. Meshkani, A novel dual-layer, gas-assisted electrospun, nanofibrous SAN4-HIPS membrane for industrial textile wastewater treatment by direct contact membrane distillation (DCMD), J. Water Proc. Eng. 36 (2020), 101315, https://doi.org/10.1016/j.jwpe.2020.101315.
[102] Q. Zhang, X. Wang, J. Fu, R. Liu, H. He, J. Ma, et al., Electrospinning of ultrafine conducting polymer composite nanofibers with diameter less than 70 nm as high sensitive gas sensor, Materials 11 (2018) 1744, https://doi.org/10.3390/ma11091744.
[103] P.L. Sóti, K. Bocz, H. Pataki, Z. Eke, A. Farkas, G. Verreck, et al., Comparison of spray drying, electroblowing and electrospinning for preparation of Eudragit E and itraconazole solid dispersions, Int. J. Pharm. 494 (2015) 23–30, https://doi.org/10.1016/j.ijpharm.2015.07.076.
[104] X. Shi, W. Zhou, D. Ma, Q. Ma, D. Bridges, Y. Ma, et al., Electrospinning of nanofibers and their applications for energy devices, J. Nanomater. 2015 (2015) 1–20, https://doi.org/10.1155/2015/140716.
[105] B. Ksapabutr, M. Panapoy, Fundamentals of electrospinning and safety, in: Metal Oxide-Based Nanofibers and Their Applications, Elsevier, 2022, pp. 3–30, https://doi.org/10.1016/B978-0-12-820629-4.00004-7.
[106] J.L. Daristotle, A.M. Behrens, A.D. Sandler, P. Kofinas, A review of the fundamental principles and applications of solution blow spinning, ACS Appl. Mater. Interfaces 8 (2016) 34951–34963, https://doi.org/10.1021/acsami.6b12994.
[107] X. hai Zhou, L. Li, Z. huan Li, L. lan Fan, W. min Kang, B. wen Cheng, The preparation of continuous CeO2/CuO/Al2O3 ultrafine fibers by electroblowing spinning (EBS) and its photocatalytic activity, J. Mater. Sci. Mater. Electron. 28 (2017) 12580–12590, https://doi.org/10.1007/s10854-017-7082-4.
[108] Y. Liu, C. Jia, H. Zhang, H. Wang, P. Li, L. Jia, et al., Free-standing ultrafine nanofiber papers with high $PM_{0.3}$ mechanical filtration efficiency by scalable blow and electro-blow spinning, ACS Appl. Mater. Interfaces 13 (2021) 34773–34781, https://doi.org/10.1021/acsami.1c04253.
[109] L. Zhang, P. Kopperstad, M. West, N. Hedin, H. Fong, Generation of polymer ultrafine fibers through solution (air-) blowing, J. Appl. Polym. Sci. 114 (2009) 3479–3486, https://doi.org/10.1002/app.30938.
[110] A.S. Niknejad, S. Bazgir, A. Sadeghzadeh, M.M.A. Shirazi, Evaluation of a novel and highly hydrophobic acrylonitrile-butadiene-styrene membrane for direct contact membrane distillation: electroblowing/air-assisted electrospraying techniques, Desalination 500 (2021), 114893, https://doi.org/10.1016/j.desal.2020.114893.
[111] M. Peng, Q. Sun, Q. Ma, P. Li, Mesoporous silica fibers prepared by electroblowing of a poly(methyl methacrylate)/tetraethoxysilane mixture in N,N-dimethylformamide, Microporous Mesoporous Mater. 115 (2008) 562–567, https://doi.org/10.1016/j.micromeso.2008.02.035.
[112] J. Paajanen, L. Pettilä, S. Lönnrot, M. Heikkilä, T. Hatanpää, M. Ritala, et al., Electroblown titanium dioxide and titanium dioxide/silicon dioxide submicron fibers with and without titania nanorod layer for strontium(II) uptake, Chemical Engineering Journal Advances 13 (2023), 100434, https://doi.org/10.1016/j.ceja.2022.100434.
[113] C. Burger, B.S. Hsiao, B. Chu, Nanofibrous materials and their applications, Annu. Rev. Mater. Res. 36 (2006) 333–368, https://doi.org/10.1146/annurev.matsci.36.011205.123537.
[114] A.J., . J.B.U.P, Bryner MA, Electroblowing Web Formation Process, 20060138710, 2006.
[115] I.C. Um, D. Fang, B.S. Hsiao, A. Okamoto, B. Chu, Electro-spinning and electro-blowing of hyaluronic acid, Biomacromolecules 5 (2004) 1428–1436, https://doi.org/10.1021/bm034539b.
[116] M. Choi, J. Kim, Development of coaxial air-blown electrospinning process for manufacturing non-woven nanofiber. II. Intelligent modeling, Fibers Polym. 20 (2019) 1883–1892, https://doi.org/10.1007/s12221-019-1094-z.
[117] M. Choi, J. Kim, Development of coaxial air-blown electrospinning process for manufacturing non-woven nanofiber. I. Morphology changes in non-woven nanofiber, Fibers Polym. 20 (2019) 1601–1607, https://doi.org/10.1007/s12221-019-1058-3.
[118] H.-Y. Hsiao, C.-M. Huang, Y.-Y. Liu, Y.-C. Kuo, H. Chen, Effect of air blowing on the morphology and nanofiber properties of blowing-assisted electrospun

polycarbonates, J. Appl. Polym. Sci. (2011), https://doi.org/10.1002/app.35599 n/a-n/a.
[119] X. Zhou, L. Li, Z. huan Li, L. lan Fan, W. min Kang, B. wen Cheng, The preparation of continuous CeO2/CuO/Al2O3 ultrafine fibers by electro-blowing spinning (EBS) and its photocatalytic activity, J. Mater. Sci. Mater. Electron. 28 (2017) 12580–12590, https://doi.org/10.1007/s10854-017-7082-4.
[120] Y.-X. Zhao, X.-H. Zhou, L. Li, W. Xu, W.-M. Kang, B.-W. Cheng, Preparation of porous CeO 2/CuO/Al 2 O 3 fibers via electro-blown spinning method, Mater. Lett. 164 (2016) 460–463, https://doi.org/10.1016/j.matlet.2015.11.033.
[121] X. Zhou, J. Ju, Z. Li, M. Zhang, N. Deng, B. Cheng, et al., Design and fabrication of flexible mesoporous Si-doped Al2O3 ultrafine fibers by electro-blow spinning (EBS) technique, Ceram. Int. 43 (2017) 9729–9737, https://doi.org/10.1016/j.ceramint.2017.04.148.
[122] W. Zheng, X. Wang, Effects of cylindrical-electrode-assisted solution blowing spinning process parameters on polymer nanofiber morphology and microstructure, E-Polymers 19 (2019) 190–202, https://doi.org/10.1515/epoly-2019-0020.
[123] A.S. Safigianni, A.I. Spyridopoulos, V.L. Kanas, Electric and magnetic field measurements in a high voltage center, in: 2011 10th International Conference on Environment and Electrical Engineering, IEEE, 2011, pp. 1–4, https://doi.org/10.1109/EEEIC.2011.5874771.
[124] X. Zhou, J. Ju, Z. Li, M. Zhang, N. Deng, B. Cheng, et al., Design and fabrication of flexible mesoporous Si-doped Al2O3 ultrafine fibers by electro-blow spinning (EBS) technique, Ceram. Int. 43 (2017) 9729–9737, https://doi.org/10.1016/j.ceramint.2017.04.148.
[125] J. He, Y. Lian, X. Zhang, Y. Wu, R. Liu, Mass preparation of nanofibers by high pressure air-jet split electrospinning: effect of electric field, J. Polym. Sci. B Polym. Phys. 52 (2014) 993–1001, https://doi.org/10.1002/polb.23519.
[126] M. Pokorny, V. Rassushin, L. Wolfova, V. Velebny, Increased production of nanofibrous materials by electroblowing from blends of hyaluronic acid and polyethylene oxide, Polym. Eng. Sci. 56 (2016) 932–938, https://doi.org/10.1002/pen.24322.
[127] A. Raksa, P. Numpaisal, Y. Ruksakulpiwat, The effect of humidity during electrospinning on morphology and mechanical properties of SF/PVA nanofibers, Mater. Today Proc. 47 (2021) 3458–3461, https://doi.org/10.1016/j.matpr.2021.03.459.
[128] W. Zheng, W. Zheng, X. Wang, The effect of electric field on nanofibers preparation in cylindrical-electrode-assisted solution blowing spinning, Autex Res. J. 20 (2020) 497–505, https://doi.org/10.2478/aut-2019-0026.
[129] R.M. Nezarati, M.B. Eifert, E. Cosgriff-Hernandez, Effects of humidity and solution viscosity on electrospun fiber morphology, Tissue Eng. C Methods 19 (2013) 810–819, https://doi.org/10.1089/ten.tec.2012.0671.
[130] J. Ju, N. Deng, D. Zhang, J. Yan, L. Li, W. Kang, et al., Facile construction of PCNF& CNT composite material by one-step simultaneous carbonization and chemical vapor deposition, J. Mater. Sci. 54 (2019) 1616–1628, https://doi.org/10.1007/s10853-018-2932-x.
[131] L. Wang, N. Deng, G. Wang, J. Ju, B. Cheng, W. Kang, Constructing amino-functionalized flower-like metal–organic framework nanofibers in sulfonated poly(ether sulfone) proton exchange membrane for simultaneously enhancing interface compatibility and proton conduction, ACS Appl. Mater. Interfaces 11 (2019) 39979–39990, https://doi.org/10.1021/acsami.9b13496.
[132] M. Peng, Q. Sun, Q. Ma, P. Li, Mesoporous silica fibers prepared by electroblowing of a poly(methyl methacrylate)/tetraethoxysilane mixture in N,N-dimethylformamide, Microporous Mesoporous Mater. 115 (2008) 562–567, https://doi.org/10.1016/j.micromeso.2008.02.035.
[133] B. Démuth, D.L. Galata, E. Szabó, B. Nagy, A. Farkas, A. Balogh, et al., Investigation of deteriorated dissolution of amorphous itraconazole: description of incompatibility with magnesium stearate and possible solutions, Mol. Pharm. 14 (2017) 3927–3934, https://doi.org/10.1021/acs.molpharmaceut.7b00629.
[134] S. Sinha-Ray, Y. Zhang, A.L. Yarin, S.C. Davis, B. Pourdeyhimi, Solution blowing of soy protein fibers, Biomacromolecules 12 (2011) 2357–2363, https://doi.org/10.1021/bm200438v.
[135] Y.-X. Zhao, X.-H. Zhou, L. Li, W. Xu, W.-M. Kang, B.-W. Cheng, Preparation of porous CeO 2/CuO/Al 2 O 3 fibers via electro-blown spinning method, Mater. Lett. 164 (2016) 460–463, https://doi.org/10.1016/j.matlet.2015.11.033.
[136] J. Holopainen, M. Ritala, Rapid production of bioactive hydroxyapatite fibers via electroblowing, J. Eur. Ceram. Soc. 36 (2016) 3219–3224, https://doi.org/10.1016/j.jeurceramsoc.2016.05.011.
[137] P.L. Sóti, K. Bocz, H. Pataki, Z. Eke, A. Farkas, G. Verreck, et al., Comparison of spray drying, electroblowing and electrospinning for preparation of Eudragit E and itraconazole solid dispersions, Int. J. Pharm. 494 (2015) 23–30, https://doi.org/10.1016/j.ijpharm.2015.07.076.
[138] X. Zhou, J. Ju, Z. Li, M. Zhang, N. Deng, B. Cheng, et al., Design and fabrication of flexible mesoporous Si-doped Al2O3 ultrafine fibers by electro-blow spinning (EBS) technique, Ceram. Int. 43 (2017) 9729–9737, https://doi.org/10.1016/j.ceramint.2017.04.148.
[139] M. Pokorny, J. Novak, J. Rebicek, J. Klemes, V. Velebny, An electrostatic spinning technology with improved functionality for the manufacture of nanomaterials from solutions, Nanomater. Nanotechnol. 5 (2015) 17, https://doi.org/10.5772/60773.
[140] A. Balogh, T. Horváthová, Z. Fülöp, T. Loftsson, A.H. Harasztos, G. Marosi, et al., Electroblowing and electrospinning of fibrous diclofenac sodium-cyclodextrin complex-based reconstitution injection, J. Drug Deliv. Sci. Technol. 26 (2015) 28–34, https://doi.org/10.1016/j.jddst.2015.02.003.
[141] C.S. Kong, W.S. Yoo, K.Y. Lee, H.S. Kim, Nanofiber deposition by electroblowing of PVA (polyvinyl alcohol), J. Mater. Sci. 44 (2009) 1107–1112, https://doi.org/10.1007/s10853-008-3209-6.
[142] W. Liu, Y. Yao, Y. Lin, Q. Zhang, Electrospinning Assisted by Gas Jet for Preparing Ultrafine Poly(vinyl alcohol) Fibres multiferroic materials View project A nitro-decorated NbO-type metal-organic framework with a highly selective CO2 uptake and CH4 storage capacity View project, n.d. https://www.researchgate.net/publication/265824353.
[143] A. Balogh, T. Horváthová, Z. Fülöp, T. Loftsson, A.H. Harasztos, G. Marosi, et al., Electroblowing and electrospinning of fibrous diclofenac sodium-cyclodextrin complex-based reconstitution injection, J. Drug Deliv. Sci. Technol. 26 (2015) 28–34, https://doi.org/10.1016/j.jddst.2015.02.003.
[144] S. Sinha-Ray, M.W. Lee, S. Sinha-Ray, S. An, B. Pourdeyhimi, S.S. Yoon, et al., Supersonic nanoblowing: a new ultra-stiff phase of nylon 6 in 20–50 nm confinement, J Mater Chem C Mater 1 (2013) 3491, https://doi.org/10.1039/c3tc30248b.
[145] X. Zhou, J. Ju, N. Deng, Z. Li, W. Kang, B. Cheng, Designing of one-dimensional C/Ce-compound composite materials, Mater. Lett. 236 (2019) 34–37, https://doi.org/10.1016/j.matlet.2018.10.052.
[146] A. al Rai, E. Stojanovska, Y. Akgul, M.M. Khan, A. Kilic, S. Yilmaz, Fabrication of co-PVDF/modacrylic/SiO2 nanofibrous membrane: composite separator for safe and high performance lithium-ion batteries, J. Appl. Polym. Sci. 138 (2021), https://doi.org/10.1002/app.49835.
[147] Y. Liang, J. Ju, N. Deng, X. Zhou, J. Yan, W. Kang, et al., Super-hydrophobic self-cleaning bead-like SiO 2 @PTFE nanofiber membranes for waterproof-breathable applications, Appl. Surf. Sci. 442 (2018) 54–64, https://doi.org/10.1016/j.apsusc.2018.02.126.
[148] M. Gungor, A. Toptas, M.D. Calisir, A. Kilic, Aerosol filtration performance of nanofibrous mats produced via electrically assisted industrial-scale solution blowing, Polym. Eng. Sci. 61 (2021) 2557–2566, https://doi.org/10.1002/pen.25780.
[149] A. al Rai, E. Stojanovska, G. Fidan, E. Yetgin, Y. Polat, A. Kilic, et al., Structure and performance of electroblown PVDF-based nanofibrous electret filters, Polym. Eng. Sci. 60 (2020) 1186–1193, https://doi.org/10.1002/pen.25372.
[150] W. Zheng, C. Shi, Y. Hu, X. Wang, Y. Wang, Theoretical and experimental studies on the fabrication of cylindrical-electrode-assisted solution blowing spinning nanofibers, E-Polymers 21 (2021) 411–419, https://doi.org/10.1515/epoly-2021-0040.
[151] Y.C. Zeng, Y.-Q. Wan, C.W. Yu, J.-H. He, Controlling the air vortex twist in air-jet spinning, Textil. Res. J. 75 (2005) 175–177, https://doi.org/10.1177/0040517505075002216.
[152] X. Liu, X. Su, Research on flow field in a modified ring spinning system with the air nozzle, J. Text. Inst. 108 (2017) 489–499, https://doi.org/10.1080/00405000.2016.1171480.
[153] D. Tian, J.-H. He, Control of macromolecule chains structure in a nanofiber, Polymers 12 (2020) 2305, https://doi.org/10.3390/polym12102305.
[154] A.S. Niknejad, S. Bazgir, A. Sadeghzadeh, M.M.A. Shirazi, Styrene-acrylonitrile (SAN) nanofibrous membranes with unique properties for desalination by direct contact membrane distillation (DCMD) process, Desalination 488 (2020), 114502, https://doi.org/10.1016/j.desal.2020.114502.
[155] A.S. Niknejad, S. Bazgir, A. Sadeghzadeh, M.M.A. Shirazi, Evaluation of a novel and highly hydrophobic acrylonitrile-butadiene-styrene membrane for direct contact membrane distillation: electroblowing/air-assisted electrospraying techniques, Desalination 500 (2021), 114893, https://doi.org/10.1016/j.desal.2020.114893.
[156] A.S. Niknejad, S. Bazgir, A. Kargari, M. Barani, E. Ranjbari, M. Rasouli, A high-flux polystyrene-reinforced styrene-acrylonitrile/polyacrylonitrile nanofibrous membrane for desalination using direct contact membrane distillation, J. Membr. Sci. 638 (2021), 119744, https://doi.org/10.1016/j.memsci.2021.119744.
[157] M.M.A. Shirazi, S. Bazgir, F. Meshkani, A novel dual-layer, gas-assisted electrospun, nanofibrous SAN4-HIPS membrane for industrial textile wastewater treatment by direct contact membrane distillation (DCMD), J. Water Proc. Eng. 36 (2020), 101315, https://doi.org/10.1016/j.jwpe.2020.101315.
[158] A.S. Niknejad, S. Bazgir, M. Ardjmand, M.M.A. Shirazi, Spent caustic wastewater treatment using direct contact membrane distillation with electroblown styrene-acrylonitrile membrane, Int. J. Environ. Sci. Technol. 18 (2021) 2283–2294, https://doi.org/10.1007/s13762-020-02972-x.
[159] R. Sallakhniknezhad, M. Khorsi, A.S. Niknejad, S. Bazgir, A. Kargari, M. Sazegar, et al., Enhancement of physical characteristics of styrene–acrylonitrile nanofiber membranes using various post-treatments for membrane distillation, Membranes 11 (2021) 969, https://doi.org/10.3390/membranes11120969.
[160] S. Khoshnevisan, S. Bazgir, Treatment of dye wastewater by direct contact membrane distillation using superhydrophobic nanofibrous high-impact polystyrene membranes, Int. J. Environ. Sci. Technol. 18 (2021) 1513–1528, https://doi.org/10.1007/s13762-020-02894-8.
[161] L. Li, H. Ren, Y. Liu, X. Liu, Y. Zhao, X. Zhou, et al., Facile construction of hierarchical porous ultrafine alumina fibers (HPAFs) and its application for dye adsorption, Microporous Mesoporous Mater. 308 (2020), 110544, https://doi.org/10.1016/j.micromeso.2020.110544.
[162] R. Sallakhniknezhad, M. Khorsi, A.S. Niknejad, S. Bazgir, A. Kargari, M. Sazegar, et al., Enhancement of physical characteristics of styrene–acrylonitrile nanofiber membranes using various post-treatments

for membrane distillation, Membranes 11 (2021) 969, https://doi.org/10.3390/membranes11120969.
[163] S. Khoshnevisan, S. Bazgir, Treatment of dye wastewater by direct contact membrane distillation using superhydrophobic nanofibrous high-impact polystyrene membranes, Int. J. Environ. Sci. Technol. 18 (2021) 1513–1528, https://doi.org/10.1007/s13762-020-02894-8.
[164] A.S. Niknejad, S. Bazgir, A. Kargari, Mechanically improved superhydrophobic nanofibrous polystyrene/high-impact polystyrene membranes for promising membrane distillation application, J. Appl. Polym. Sci. 138 (2021), 50917, https://doi.org/10.1002/app.50917.
[165] A. Sadeghzadeh, S. Bazgir, M.M.A. Shirazi, Fabrication and characterization of a novel hydrophobic polystyrene membrane using electroblowing technique for desalination by direct contact membrane distillation, Sep. Purif. Technol. 239 (2020), 116498, https://doi.org/10.1016/j.seppur.2019.116498.
[166] A.S. Niknejad, S. Bazgir, A. Kargari, M. Barani, E. Ranjbari, M. Rasouli, A high-flux polystyrene-reinforced styrene-acrylonitrile/polyacrylonitrile nanofibrous membrane for desalination using direct contact membrane distillation, J. Membr. Sci. 638 (2021), 119744, https://doi.org/10.1016/j.memsci.2021.119744.
[167] A.S. Niknejad, S. Bazgir, A. Sadeghzadeh, M.M.A. Shirazi, Styrene-acrylonitrile (SAN) nanofibrous membranes with unique properties for desalination by direct contact membrane distillation (DCMD) process, Desalination 488 (2020), 114502, https://doi.org/10.1016/j.desal.2020.114502.
[168] A.S. Niknejad, S. Bazgir, A. Kargari, Desalination by direct contact membrane distillation using a superhydrophobic nanofibrous poly (methyl methacrylate) membrane, Desalination 511 (2021), 115108, https://doi.org/10.1016/j.desal.2021.115108.
[169] A.S. Niknejad, S. Bazgir, A. Sadeghzadeh, M.M.A. Shirazi, Evaluation of a novel and highly hydrophobic acrylonitrile-butadiene-styrene membrane for direct contact membrane distillation: electroblowing/air-assisted electrospraying techniques, Desalination 500 (2021), 114893, https://doi.org/10.1016/j.desal.2020.114893.
[170] W.W.F. Leung, Q. Sun, Electrostatic charged nanofiber filter for filtering airborne novel coronavirus (COVID-19) and nano-aerosols, Sep. Purif. Technol. 250 (2020), 116886, https://doi.org/10.1016/j.seppur.2020.116886.
[171] Y. Liu, C. Jia, H. Zhang, H. Wang, P. Li, L. Jia, et al., Free-standing ultrafine nanofiber papers with high $PM_{0.3}$ mechanical filtration efficiency by scalable blow and electro-blow spinning, ACS Appl. Mater. Interfaces 13 (2021) 34773–34781, https://doi.org/10.1021/acsami.1c04253.
[172] M. Shahid, B. Pourrut, C. Dumat, M. Nadeem, M. Aslam, E. Pinelli, Heavy-Metal-Induced Reactive Oxygen Species: Phytotoxicity and Physicochemical Changes in Plants, 2014, pp. 1–44, https://doi.org/10.1007/978-3-319-06746-9_1.
[173] G. Azeh Engwa, P. Udoka Ferdinand, F. Nweke Nwalo, M.N. Unachukwu, Mechanism and health effects of heavy metal toxicity in humans, in: Poisoning in the Modern World - New Tricks for an Old Dog?, IntechOpen, 2019, https://doi.org/10.5772/intechopen.82511.
[174] J. Paajanen, S. Weintraub, S. Lönnrot, M. Heikkilä, M. Vehkamäki, M. Kemell, et al., Novel electroblowing synthesis of tin dioxide and composite tin dioxide/silicon dioxide submicron fibers for cobalt(<scp>ii</scp>) uptake, RSC Adv. 11 (2021) 15245–15257, https://doi.org/10.1039/D1RA01559A.
[175] J. Paajanen, S. Lönnrot, M. Heikkilä, K. Meinander, M. Kemell, T. Hatanpää, et al., Novel electroblowing synthesis of submicron zirconium dioxide fibers: effect of fiber structure on antimony(<scp>v</scp>) adsorption, Nanoscale Adv. 1 (2019) 4373–4383, https://doi.org/10.1039/C9NA00414A.
[176] J. Luo, X. Luo, J. Crittenden, J. Qu, Y. Bai, Y. Peng, et al., Removal of antimonite (Sb(III)) and antimonate (Sb(V)) from aqueous solution using carbon nanofibers that are decorated with zirconium oxide (ZrO_2), Environ. Sci. Technol. 49 (2015) 11115–11124, https://doi.org/10.1021/acs.est.5b02903.
[177] Y. Zhang, L. Gao, N. Deng, M. Ya, H. He, W. Kang, et al., Fabrication of porous and magnetic Fe/FeNX fibers by electro-blown spinning method for efficient adsorption of Cr (VI) ions, Mater. Lett. 212 (2018) 235–238, https://doi.org/10.1016/j.matlet.2017.10.104.
[178] S. Lönnrot, J. Paajanen, V. Suorsa, W. Zhang, M. Ritala, R. Koivula, Sb-doped zirconium dioxide submicron fibers for separation of pertechnetate (TcO_4^-) from aqueous solutions, Separ. Sci. Technol. 56 (2021) 2338–2350, https://doi.org/10.1080/01496395.2020.1826967.
[179] M. Sazegar, S. Bazgir, A.A. Katbab, Preparation and characterization of water-absorbing gas-assisted electrospun nanofibers based on poly(vinyl alcohol)/chitosan, Mater. Today Commun. 25 (2020), 101489, https://doi.org/10.1016/j.mtcomm.2020.101489.
[180] R. Aminyan, S. Bazgir, Fabrication and characterization of nanofibrous polyacrylic acid superabsorbent using gas-assisted electrospinning technique, React. Funct. Polym. 141 (2019) 133–144, https://doi.org/10.1016/j.reactfunctpolym.2019.05.012.
[181] L. Cao, X. Zhou, Z. Li, K. Su, B. Cheng, Nitrogen and fluorine hybridization state tuning in hierarchical honeycomb-like carbon nanofibers for optimized electrocatalytic ORR in alkaline and acidic electrolytes, J. Power Sources 413 (2019) 376–383, https://doi.org/10.1016/j.jpowsour.2018.12.076.
[182] N. Mandakhbayar, A. El-Fiqi, K. Dashnyam, H.-W. Kim, Feasibility of defect tunable bone engineering using electroblown bioactive fibrous scaffolds with dental stem cells, ACS Biomater. Sci. Eng. 4 (2018) 1019–1028, https://doi.org/10.1021/acsbiomaterials.7b00810.
[183] H. Abdolbaghian, S. Bazgir, Fabrication and characterization of gas-assisted core-shell hydrogel nanofibers as a drug release system with antibacterial activity, Eur. Polym. J. 174 (2022), 111302, https://doi.org/10.1016/j.eurpolymj.2022.111302.
[184] K. Jiang, Y.-Z. Long, Z.-J. Chen, S.-L. Liu, Y.-Y. Huang, X. Jiang, et al., Airflow-directed in situ electrospinning of a medical glue of cyanoacrylate for rapid hemostasis in liver resection, Nanoscale 6 (2014) 7792, https://doi.org/10.1039/c4nr01412j.
[185] W. Liu, J. Ju, N. Deng, L. Wang, G. Wang, L. Li, et al., Designing inorganic-organic nanofibrous composite membrane for advanced safe Li-ion capacitors, Electrochim. Acta 337 (2020), 135821, https://doi.org/10.1016/j.electacta.2020.135821.
[186] N. Deng, W. Kang, J. Ju, L. Fan, X. Zhuang, X. Ma, et al., Polyvinyl Alcohol-derived carbon nanofibers/carbon nanotubes/sulfur electrode with honeycomb-like hierarchical porous structure for the stable-capacity lithium/sulfur batteries, J. Power Sources 346 (2017) 1–12, https://doi.org/10.1016/j.jpowsour.2017.02.022.
[187] L. Wang, J. Ju, N. Deng, B. Cheng, W. Kang, Embedding red phosphorus in hierarchical porous carbon nanofibers as anodes for lithium-ion battery, Mater. Lett. 240 (2019) 39–43, https://doi.org/10.1016/j.matlet.2018.12.103.
[188] Y. Hao, L. Wang, Y. Liang, B. He, Y. Zhang, B. Cheng, et al., Bifunctional semi-closed YF_3 -doped 1D carbon nanofibers with 3D porous network structure including fluorinating interphases and polysulfide confinement for lithium–sulfur batteries, Nanoscale 11 (2019) 21324–21339, https://doi.org/10.1039/C9NR07809F.
[189] W. Kang, L. Fan, N. Deng, H. Zhao, Q. Li, M. Naebe, et al., Sulfur-embedded porous carbon nanofiber composites for high stability lithium-sulfur batteries, Chem. Eng. J. 333 (2018) 185–190, https://doi.org/10.1016/j.cej.2017.09.134.
[190] M. Liu, N. Deng, J. Ju, L. Wang, G. Wang, Y. Ma, et al., Silver nanoparticle-doped 3D porous carbon nanofibers as separator coating for stable lithium metal anodes, ACS Appl. Mater. Interfaces 11 (2019) 17843–17852, https://doi.org/10.1021/acsami.9b04122.
[191] N. Deng, J. Ju, J. Yan, X. Zhou, Q. Qin, K. Zhang, et al., CeF_3 -doped porous carbon nanofibers as sulfur immobilizers in cathode material for high-performance lithium–sulfur batteries, ACS Appl. Mater. Interfaces 10 (2018) 12626–12638, https://doi.org/10.1021/acsami.7b19746.
[192] J. Ju, H. Zhao, W. Kang, N. Tian, N. Deng, B. Cheng, Designing MnO2 & carbon composite porous nanofiber structure for supercapacitor applications, Electrochim. Acta 258 (2017) 116–123, https://doi.org/10.1016/j.electacta.2017.10.094.
[193] F.-L. Zhou, R.-H. Gong, I. Porat, Mass production of nanofibre assemblies by electrostatic spinning, Polym. Int. 58 (2009) 331–342, https://doi.org/10.1002/pi.2521.
[194] Y. Liu, C. Jia, P. Li, H. Zhang, L. Jia, L. Yu, et al., Mass production of hierarchically designed engine-intake air filters by multinozzle electroblow spinning, Nano Lett. 22 (2022) 4354–4361, https://doi.org/10.1021/acs.nanolett.2c00704.
[195] G. Xu, X. Chen, Z. Zhu, P. Wu, H. Wang, X. Chen, et al., Pulse gas-assisted multi-needle electrospinning of nanofibers, Adv. Compos. Hybrid Mater. 3 (2020) 98–113, https://doi.org/10.1007/s42114-019-00129-0.
[196] M. Wojasiński, J. Goławski, T. Ciach, Blow-assisted multi-jet electrospinning of poly-L-lactic acid nanofibers, J. Polym. Res. 24 (2017) 76, https://doi.org/10.1007/s10965-017-1233-4.